Kaunas University of Technology

Faculty of chemical technology

Synthesis of divalent organic cations and their application in highly efficient and stable perovskite solar cells

Master's Final Degree Project

Raminta Skačkauskaitė

Project author

Snr researcher Dr. Marytė Daškevičienė

Supervisor

Kaunas, 2021

Kaunas University of Technology

Faculty of chemical technology

Synthesis of divalent organic cations and their application in highly efficient and stable perovskite solar cells

Master's Final Degree Project

Applied chemistry (6211CX014)

Raminta Skačkauskaitė

Project author

Snr researcher Dr. Marytė Daškevičienė

Supervisor

Chief researcher Dr. Kasparas Rakštys

Consultant

Snr researcher Dr. Jūratė Simokaitienė

Reviewer

Kaunas, 2021

Kaunas University of Technology

Faculty of chemical technology

Raminta Skačkauskaitė

Synthesis of divalent organic cations and their application in highly efficient and stable perovskite solar cells

Declaration of Academic Integrity

I confirm the following:

1. I have prepared the final degree project independently and honestly without any violations of the copyrights or other rights of others, following the provisions of the Law on Copyrights and Related Rights of the Republic of Lithuania, the Regulations on the Management and Transfer of Intellectual Property of Kaunas University of Technology (hereinafter – University) and the ethical requirements stipulated by the Code of Academic Ethics of the University;

2. All the data and research results provided in the final degree project are correct and obtained legally; none of the parts of this project are plagiarised from any printed or electronic sources; all the quotations and references provided in the text of the final degree project are indicated in the list of references;

3. I have not paid anyone any monetary funds for the final degree project or the parts thereof unless required by the law;

4. I understand that in the case of any discovery of the fact of dishonesty or violation of any rights of others, the academic penalties will be imposed on me under the procedure applied at the University; I will be expelled from the University and my final degree project can be submitted to the Office of the Ombudsperson for Academic Ethics and Procedures in the examination of a possible violation of academic ethics.

Raminta Skačkauskaitė, *Confirmed electronically*

Skačkauskaitė, Raminta. Synthesis of divalent organic cations and their application in highly efficient and stable perovskite solar cells. Master's Final Degree Project / supervisor Snr researcher Dr. Marytė Daškevičienė; Faculty of chemical technology, Kaunas University of Technology.

Study field and area (study field group): chemistry, physical sciences.

Keywords: solar cell, perovskite, 2D perovskite, 3D perovskite, divalent organic cations, efficiency, stability.

Kaunas, 2021. 55 p.

Summary

Solar cells may provide our future with clean, cheap, and infinite energy. Nowadays, the most used solar cells are heavy, bulky, and manufactured pure silicon material requires a lot of expenses. However, different solar cells are being researched and studied more such as perovskite solar cells. Perovskite solar cells were discovered only a decade ago and they have already exceeded the efficiency of older generation solar cells. They are lightweight, durable, flexible and they do not require high fabrication costs. Nevertheless, they still cannot be used industrially due to their low moisture stability.

Three-dimensional perovskite solar cells are typical perovskite solar cells that have high power conversion efficiency, yet are sensitive to humid environment and degrade fast. Two-dimensional perovskite solar cells, on the other hand, have quite low power conversion efficiency but their structure lets them incorporate organic spacer cations that could provide various properties. Integrating certain organic cations in two-dimensional perovskite and mixing them with three-dimensional perovskite could lead to the compositions with tunable properties and synergistic effect. Two-dimensional Ruddlesden-Popper phase consists of organic monoammonium cations, and it was the first to be studied, while Dion-Jacobson phase consists of organic diammonium cations which is relatively poor studied. Dion-Jacobson organic cations have an advantage over Ruddlesden-Popper cations – strongly covalently bonded perovskite fragments. Moreover, by having fluorine atoms in the cation structure, it is expected to enhance the moisture stability of perovskite compositions as these atoms are known to have water repellent properties.

First of all, isomeric organic *o*, *m*, *p*-phenylenediethanamonium iodide cations for Dion-Jacobson phase were synthesised and only *p*-isomer was successfully integrated in two-dimensional perovskite structure to show a power conversion efficiency of 13.54 %, while *o*- and *m*-cations were not able to form Dion-Jacobson phase most probably due to the steric hindrance. Furthermore, synthesised isomeric cations having free ammonium groups were used as passivating agents on three-dimensional perovskite and solar cell having *o*-cation as an extra passivation layer showed the power conversion efficiency of over 23 % with increased moisture stability after 1000 hours in humid environment. Lastly, (perfluoro-1,4-phenylene)dimethanamonium and (perfluoro-1,4-phenylene)diethanamonium iodide cations were synthesised in order to increase the hydrophobicity of such systems. Further synthesis of divalent organic cations and their perovskite composition modification is essential in order to enhance the performance and stability of mixed perovskite-based solar cells.

Skačkauskaitė, Raminta. Organinių dvivalenčių katijonų sintezė ir pritaikymas efektyviems bei stabiliems perovskitų saulės elementams. Magistro baigiamasis projektas / vadovė v. m. d. dr. Marytė Daškevičienė; Kauno technologijos universitetas, Cheminės technologijos fakultetas.

Studijų kryptis ir sritis (studijų krypčių grupė): chemija, fiziniai mokslai.

Reikšminiai žodžiai: saulės elementas, perovskitas, 2D perovskitas, 3D perovskitas, organiniai dvivalenčiai katijonai, efektyvumas, stabilumas.

Kaunas, 2021. 55 p.

Santrauka

Iš saulės elementų galima gauti ekonomišką, aplinkai draugišką ir nesibaigiančią energiją. Šiomis dienomis dažniausiai naudojami saulės elementai yra sunkūs, masyvūs, o itin švarus silicis reikalauja daug gryninimo išlaidų. Perovskitiniai saulės elementai pradėti tyrinėti visai neseniai, prieš maždaug dešimtmetį, o jų energijos konversijos efektyvumas jau pasiekė ankstesnės kartos saulės elementus. Perovskitiniai saulės elementai yra palyginamai lengvi ir lankstūs, o jų gamybos procesas yra pigus. Deja, šiuo metu jie vis dar negali būti komercializuoti bei prieinami kiekvienam žmogui, nes pasižymi žemu stabilumu atmosferinėje aplinkoje.

Perovskitiniai saulės elementai tridimensinių perovskitų pagrindu, arba įprasti perovskitiniai saulės elementai, pasižymi aukštu energijos konversijos efektyvumu, bet yra jautrūs drėgmei ir greitai degraduoja aplinkoje. Dvidimensiniai perovskitiniai saulės elementai šiuo atveju turi žemesnį energijos konversijos efektuvumą, bet dėl struktūros ypatybių juose galima integruoti organinius katijonus, o tai atveria galimybes įvairių savybių modifikavimui. Taigi, jungiant tridimensinius perovskitus su tam tikru funkcionalumu pasižyminčiais, organinių katijonų pagrindu suformuotais, dvidimensiniais gali būti gaunamos mišrios perovskitų kompozicijos ir taip išsprendžiamos esamos stabilumo problemos bei pasiektas sinerginis efektas. Ruddlesden-Popper dvidimensinių perovskitų fazė buvo pradėta tyrinėti pirmoji, o ji sudaroma iš monoamonio katijoninių prekursorių, tuo tarpu Dion-Jacobson fazė – dar visiškai naujas tyrimų objektas mokslo pasaulyje. Dion-Jacobson fazė sudaryta iš diamonio katijonų, o tai suteikia privalumą lyginant su Ruddlesden-Popper analogais – stipresnėmis kovalentinėmis jungtimis surišti perovskitų fragmentai. Taip pat, yra žinoma, kad fluoro atomai pasižymi hidrofobinėmis savybėmis, taigi naudojant fluorintus katijonus dvidimensinių perovskitų formavimui yra tikimasi pagerinti tokių kompozicijų stabilumą atmosferinėje aplinkoje. Šiame darbe siekiama susintetinti organinius dvivalenčius katijonus Dion-Jacobson dvidimensinių perovskitų formavimui bei juos panaudoti perovskitinių saulės elementų konstravimui, norint pasiekti geresnį stabilumą ir efektyvumą.

Šiame darbe pirmiausia susintetinti izomeriniai dvivalenčiai organiniai *o, m, p*-fenilendietanamonio jodido katijonai, o panaudojant *p*-katijoną buvo sėkmingai suformuotas dvidimensinis perovskitas, kurį panaudojus saulės elemento konstravime buvo pasiektas 13,54 % energijos konversijos efektyvumas, tuo tarpu panaudojus *o*- ir *m*-katijonus dvidimensinių perovskitų suformuoti nepavyko dėl sterinių trukdžių. Šie katijonai taip pat buvo panaudoti kaip laisvas amonio grupes turintys pasyvavimo agentai, šiuo tikslu ant tridimensinio perovskito sluoksnio buvo formuojamas susintetintų izomerų sluoksnis, o geriausius rezultatus pademonstravo *o*-katijonu pasyvuotas saulės elementas, kuris pasiekė 23 % energijos konversijos efektyvumą bei pasižymėjo pagerėjusiu stabilumu testuojant 1000 valandų drėgnoje aplinkoje. Taip pat, buvo susintetinti (perfluoro-1,4-

fenilen)dimetanamonio ir (perfluoro-1,4-fenilen)dietanamonio jodido katijonai siekiant padidinti jais funkcionalizuotų perovskitinių kompozicijų hidrofobiškumą. Tolimesnė dvivalenčių organinių katijonų sintezė bei jų pagrindų suformuotų perovskitų modifikacijų tyrimai yra reikalingi norint pagerinti mišrių perovskitų pagrindu veikiančių saulės elementų savybes.

Table of contents

List of schemes

List of figures

List of tables

List of abbreviations

2D – two-dimensional

3D – three-dimensional

BA – butylammonium

CB – conduction band

CIGS – copper indium gallium selenide

CZTS – copper zinc tin sulphide

DJ – Dion-Jacobson

DMSO – dimethyl sulfoxide

DSSC – dye-sensitised solar cell

ESI – electrospray ionisation

ETL – electron transport layer

FF – fill factor

HOMO – highest occupied molecular orbital

HTL – hole transport layer

$I_{MP/MAX}$ – current density at maximum power

I_{SC} – short-circuit current

I-V – current density-voltage

MA – methylammonium

MPPT – maximum power point tracing

MS – mass spectrometry

NMR – nuclear magnetic resonance

OPV – organic photovoltaic

PCE – power conversion efficiency

PDA – propane-1,3-diammonium

PEA – phenylethyl ammonium

PEDOT:PSS - poly(3,4-ethylenedioxythiophene):polystyrene sulfonate

P_{MAX} – the maximum output power (or maximum power point)

PSC – perovskite solar cell

PTAA – poly(triaryl amine)

RH – relative humidity

RP – Ruddlesden-Popper

TCO – transparent conductive oxide

TFA – trifluoroacetic acid

THF – tetrahydrofuran

UV – ultraviolet (light)

VB – valence band

$V_{MP/MAX}$ – voltage at maximum power

V_{OC} – open-circuit voltage

Vis – visible (light)

XRD – X-ray diffraction

η – solar energy conversion efficiency

Introduction

Solar cells are electrical devices that convert the energy of sunlight into electricity, and they may provide infinite energy. It is predicted that the sun will cease to exist in 2 billion years, therefore it will most likely be a source for electricity production for an incredibly long time. Furthermore, it is a renewable, environmentally and economy friendly energy. Nowadays, polycrystalline silicon is used to make a vast majority of solar cells as it provides high power conversion efficiency (PCE). However, the modules are bulky, stringent, and require high-priced manufactured pure silicon material limiting the global transition to a carbon-free energy production [1,2].

Other materials could be used and modified to make efficient, durable, yet flexible (that would be able to endure strain without being permanently damaged) and lightweight solar cells. Perovskite-based solar cells (PSCs) are made of economical and abundant precursors, as well as they are comparably light and resilient, hence they could be used for mass production and markedly reduce the fabrication costs. In 2009, PSCs were known to have reached 3.8% of PCE and soon after it became the centre of attention in photovoltaics due to notable properties. Up to date, certified PCE of PSCs has skyrocketed to over 25% [3–6]. Nevertheless, the most important issue is that three-dimensional (3D) hybrid lead halide perovskite light absorber may not be used industrially due to their low stability and decomposition in humid environment. Due to this fact it is necessary to stabilize the crystal phase of 3D perovskites and this problem could be resolved by introducing new components into the system. 3D perovskites decompose in an ambient environment in a very short time, on the other hand, two-dimensional (2D) perovskites show a relatively higher moisture resistance, yet low PCE. Therefore, by employing hydrophobic bifunctional organic cations leading to combined 2D/3D perovskite systems it is expected to increase moisture stability and maintain or increase PCE [7].

The aim of the project: to synthesize new divalent organic cations and incorporate them into mixed 2D/3D perovskite compositions leading to the solar cells with improved stability and efficiency.

The main tasks of the project:

1. Synthesize designed divalent organic cations with reactive ammonium groups with a regard to use them for perovskite film fabrication.

2. Characterization of synthesised cations-based perovskite films used in perovskite solar cells.

3. Analyse and compare the power conversion efficiency and stability properties of synthesised divalent organic cations integrated 2D/3D perovskite solar cells.

1. Literature review

1.1. Solar cells, their types and function

Solar cells are photovoltaic applications that have the ability to convert the energy of light into electricity by absorbing photons from the rays of sun providing power for smallest calculators up to space installations. In theory, from a 100% of sunlight, only around 31% may be converted to electricity by a solar cell due to the energy conversion into heat and reflection [8]. Even though lots of energy from sunlight do not hit the surface of the Earth, solar energy is still our future for many reasons, and it has more advantages compared to other sources of energy. Solar energy does not produce pollution, compared to fossil fuels which leave a detrimental impact for environment. Fossil fuels are limited resources, while solar power is infinite. Moreover, solar cells continue to increase in efficiency and are able to generate more electricity as new developments are made. Compared to other renewable sources of energy, solar cells are more easily accessible and available to consumers since it is difficult to have access to a wind turbine or a hydroelectric power plant for a regular person [9].

Classification of solar cells

Classification of solar cells is typically determined by the materials that were used to fabricate them or by the time when they were first fabricated.

First generation solar cells are still the most common and commercially available consisting of multicrystalline silicon. Such solar cells need to have >99% pure silicon which requires a lot of expenses for manufacturing process, however, theoretically it can reach up to 33% power conversion efficiency (PCE) [10–12].

The second generation solar cells were developed due to high cost of the first generation solar cells. These solar cells were developed around 1990s and 2000s and they are way cheaper compared to the first generation, yet PCE varies around 10-15%. Record PCE of 23% was reached by copper indium gallium selenide (CIGS) thin-film semiconductors. It is predicted that CIGS thin-film solar cells could theoretically reach 33% in the near future. Second generation solar cells also include cadmium telluride (CdTe), gallium arsenide (GaAs), polycrystalline silicon and amorphous silicon (a-Si:H) [10, 11, 13, 14].

The third generation was distinct from the two above, as mostly organic semiconductors were used and novel approaches were taken. The main goal was to create low-cost, high efficiency thin-film and bendable solar cells. Third generation solar cells include dye-sensitised solar cells (DSSCs), organic photovoltaics (OPVs), quantum dot solar cells, copper zinc tin sulphide (CZTS), and perovskite solar cells (PSCs). PCE in third generation solar cells usually range from 15% to 20%, however a new record was reached in 2020 with reported PSC certified PCE of 25.2%. The appearance of all three generation solar cells is shown in figure **1.1.** [6, 10, 11, 15–17].

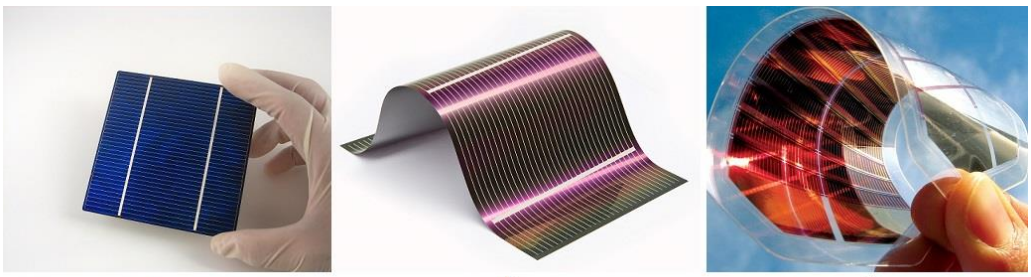

a b c

Figure 1.1. Illustration and their appearance of a) first generation solar cell; b) second generation solar cell; c) third generation solar cell. Source [12,17]

Characteristics of solar cells

To determine the metrics of a solar cell, such as PCE, current-voltage (*I-V*) measurements are implemented (figure **1.2.**). Used characteristics are:

$I_{MP/MAX}$ – current density at maximum power;
$V_{MP/MAX}$ – voltage at maximum power;
P_{MAX} – the maximum output power (or maximum power point);
I_{SC} – short-circuit current ;
V_{OC} – open-circuit voltage;
FF – fill factor;
η – solar energy conversion efficiency.

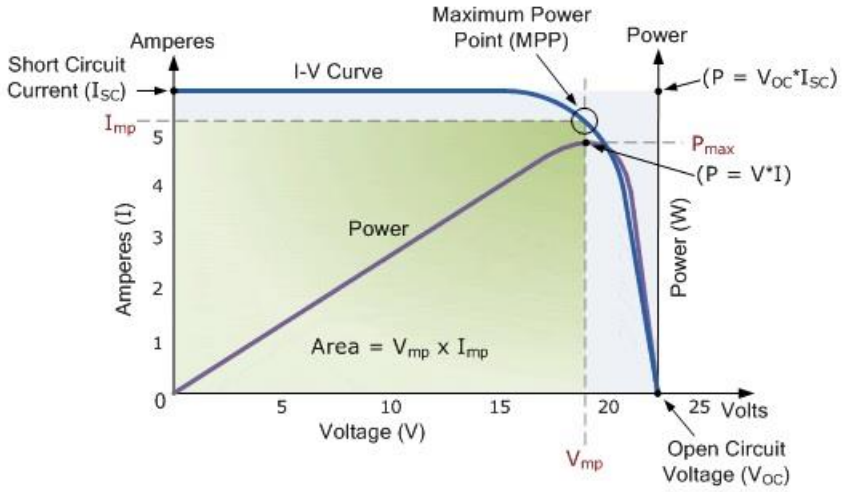

Figure 1.2. Characteristic *I-V* curve of a solar cell. Source [18]

I_{SC} is a current through a solar cell when the voltage is equal to 0, while V_{OC} is a voltage applicable from a solar cell and it takes place when current is equal to 0. FF is a parameter that evaluates the deviation of the measured solar cell efficiency from the theoretical maximum power output of the cell. It is characterized and determined as the ratio of the maximum power (P_{MAX}) to the external I_{SC} and V_{OC} values [18–20]. The efficiency η of a solar cell is defined by the proportion of electrical energy acquired and converted from a solar cell to sunlight energy that reached the cell.

1.2. Perovskite solar cells

Perovskite solar cells fall into the class of third generation photovoltaic technology. Discovered just a decade ago their PCE keeps going higher at a very fast rate, compared to other solar cells. Perovskite solar cells emerged from DSSCs, however the efficiency of DSSC is quite moderate and limited [21], while PSC have appeared as one of the most remarkable technology in terms of PCE. As a result, the researchers have shown exceptional interest in PSC. Moreover, properties such us semitransparency, flexibility, lightness of weight are treasured in PSC. Nevertheless, there are concerns about instability and raising demand not just for industrial use but also for an average household, which could significantly benefit from them. These issues must be resolved for PSCs entering the market.

Perovskite

Perovskite was firstly described by chemical formula of $CaTiO_3$, as known as calcium titanium oxide or calcium titanate, and it was discovered by German scientist Gustav Rose in 1839 in the Ural Mountains, then named in honour of Russian mineralogist Count Lev Alekseevich Perovski. Perovskite systems can be classified into inorganic oxide perovskites and halide perovskites. The latter is sorted into alkali-halide perovskites and organic-inorganic metal halide perovskites [22].

ABX_3 is the generic chemical formula used to describe the organic-inorganic metal halide perovskite materials – A stands for a large organic cation, B stands for a small metal cation and X is a halogen anion (figure **1.3.**). Perovskite properties as long-range ambipolar charge transport, high dielectric constant, high-absorption coefficient made these materials in the spotlight in use for photovoltaic applications [23].

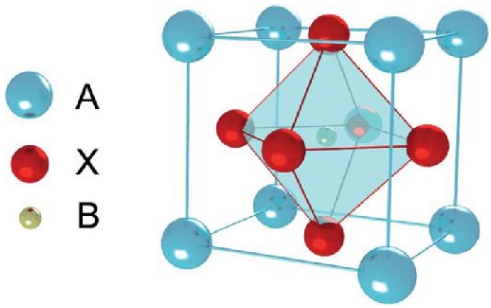

Figure 1.3. Schematic representation of ABX_3 perovskite structure, where A is a large cation, B is a small cation and X is an anion. Source [23]

Structures of perovskite solar cells

There are three typical PSCs structures: the mesoporous structure, the planar heterojunction structure, and the inverted planar heterojunction structure. The most usual configuration consists of glass/transparent conductive oxide (TCO)/blocking layer (which is also an electron transport layer (ETL))/perovskite (sunlight absorber layer)/hole transport layer (HTL)/gold (Au). There are other configurations where mesoporous layer is added on top of a blocking layer and fused with perovskite. Moreover, an inverted structure – where ETL is swapped with HTL [23].

Perovskite absorbs the sunlight and generates charges being the electron and hole pairs which diffuse and get separated through electron and hole selective contacts, respectively. In mesoporous

nanostructure the perovskite is introduced inside a mesoporous metal oxide scaffold and an extra layer of perovskite is fabricated on top. Hole transport layer (HTL) is in direct contact with the metal electrode, which can be either gold or silver (less likely aluminium and carbon materials). HTL is responsible for efficient charge extraction and spiro-OMeTAD is the most commonly used HTL material, as there are other candidates like poly(triaryl amine) (PTAA), poly(3,4-ethylenedioxythiophene):polystyrene sulfonate (PEDOT:PSS) and many others [24]. Similarly, ETL is an electron transport layer or hole blocking layer, where TiO_2 and SnO_2 are usually used for mesoporous and planar architectures, respectively. Finally, HTL and ETL are placed close to the electrodes/metals: cathode and anode (figure **1.4.**).

Figure 1.4. Three typical structures of a perovskite solar cell: a) the mesoporous structure, b) the planar heterojunction structure, c) the inverted planar heterojunction structure. Source [23]

Mechanism of function

When sunlight reaches the PSC, the basic working principle could be divided in several actions (figure **1.5.**): 1) the perovskite layer absorbs the photons and so the electron jumps from valence band (VB) to conduction band (CB), the hole is created as electron leaves the VB; 2) the photogenerated electron from perovskite CB transfers to TiO_2 CB, the electron transfers to an electrode (anode) and from there the photocurrent is initiated as it reaches another electrode (cathode); 3) positive charge or a hole is injected into the highest occupied molecular orbital (HOMO) of an HTL from which they reach cathode.

Unwanted mechanism and actions can take place as well: 4) recombination of photogenerated charge carriers, as well as 5) electron regression from TiO_2 layer back to the VB of perovskite; 6) positive charge regression from perovskite VB to HTL or even charge recombination at the TiO_2 or HTL interface. These unwanted processes need to happen slower than desirable mechanisms such as charge generation, separation, and extraction to obtain high PCE. Understanding inner mechanisms of a PSC is essential to optimize and improve PCE and other properties [25].

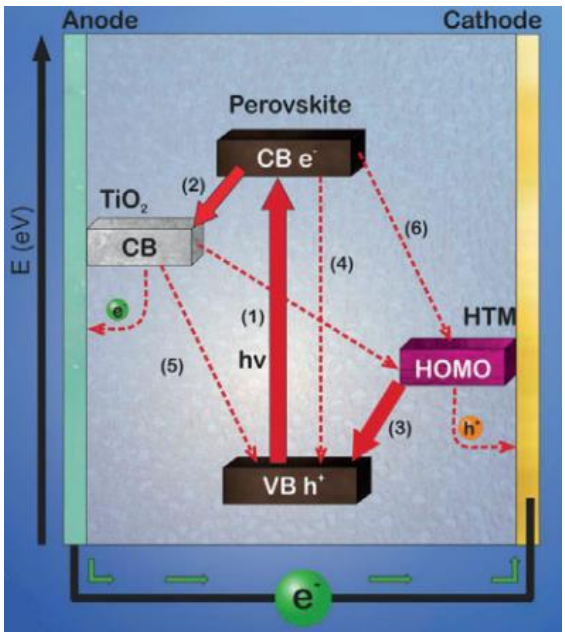

Figure 1.5. Energy levels and electron/hole-transfer processes in a perovskite solar cell. Source [25]

1.3. Two-dimensional perovskite solar cells

Solar cells that contain two-dimensional (2D) perovskites yet have still to advance more and increase the PCE to catch up with other types of PSCs, for instance, three-dimensional (3D) PSCs. Despite comparatively lower PCE, 2D PSCs have unique properties and advantages that make them valuable for the researchers. In addition to this, 2D perovskites have different functions in a solar cell: 2D perovskites can act as the primary light absorber or as a capping layer, even a passivating layer or also take place in a mixed 2D/3D perovskite solar cell absorber [26].

Two-dimensional perovskite structure

The first report on 2D perovskites was done quite recently by I. Smith et al., in 2014, with only 4.7% of PCE and up to date it already amounts to 19.3% of PCE as claimed in an article by Y. Huang et al. [27, 28]. That is a tremendous change in a very short time, which indeed shows how much potential they hold for future investigations. Furthermore, they have long term durability, stability towards ambient humidity and light exposure, improved processability and high chemical versatility. It is obvious that these properties highlight how unique 2D perovskites are and how many possibilities they hold.

2D perovskites have the ability to integrate quite large, not very volatile and mostly hydrophobic organic cations in their structure. That is an enormous benefit and can improve the whole system within and change the properties. For instance, thermal and chemical stability can also be enhanced within the solar cell. Likewise, such competence of a 2D perovskite can bring out almost infinite properties to a PSC, as a huge diversity of organic cations or even diverse metals and halides have the possibility to be merged, putted in different order and sequence [26].

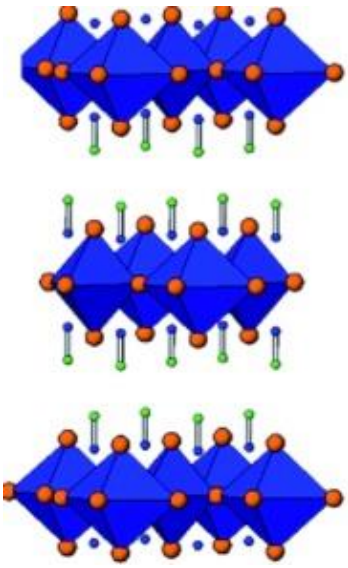

Figure 1.6. 2D perovskite crystal structure having formula of $(CH_3NH_3)_2PbI_4$: Blue sphere is the N and green sphere is the C. Halogens are represented by orange spheres. The large blue figure is presented as the MX_6 (where M equals to Pb, Sn and Cu; X equals to I and Br). Source [29]

2D perovskites are made out of one or numerous inorganic sheets that are jammed between organic spacers, which are held together by Columbic forces. The general formula for 2D perovskites is $R_2A_{n-1}B_nX_{3n+1}$ where B is a metal cation, X is a halide, R represents a large organic cation that only acts as a spacer between the inorganic sheets and n represents the quantity of inorganic layers that are put together (figure **1.6.**) [29, 30].

Organic cations in two-dimensional perovskites

As mentioned before, large organic cations can be integrated into the structure to make 2D halide perovskites. For instance, these cations could be phenylethyl ammonium with a general formula of $C_6H_5(CH_2)_2NH_3^+$ (PEA^+) and butylammonium that goes by the formula of $C_4H_9NH_3^+$ (BA^+). Just by adding these organic cations, they can bring out environmental stability within 2D halide perovskite material. Actually, PEA_2PbI_4 was crucial for defining optoelectronic and structural properties of 2D perovskite class. It was developed in the 1990s and it still is one of the most researched materials. Moreover, 2D perovskites usually have a high exciton binding energy and a great bandgap, which is noticed in PEA_2PbI_4 as well. This leads to other excellent properties for a 2D PSC: high electroluminescence, photoluminescence quantum yield, strong optical non-linearity etc [30, 31].

The flexibility of a 2D perovskite structure gives a wide scope for component exploration, exclusively by choosing a variety of R organic cations. The examples of these cations studied before are shown in figure **1.7.**

In addition, quasi 2D perovskites have analogous structure to 2D perovskites only that it is made of more layers. Quasi 2D perovskites can have long alkyl chain cations in the layered structure, which helps to push away the moisture and boosts up the stability. When PEA^+ is mixed with any other smaller cation, for instance methylammonium (MA^+), quasi-2D perovskite is obtained [30].

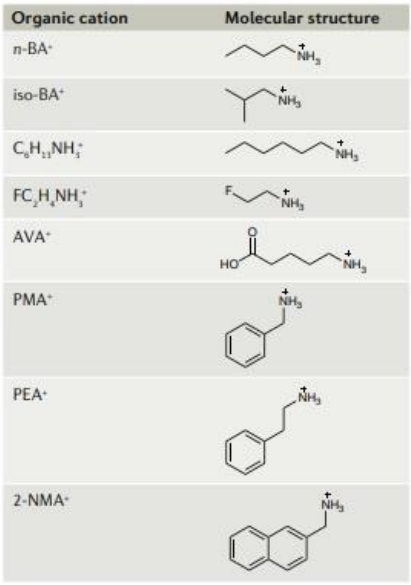

Figure 1.7. Organic cations that were incorporated into 2D perovskites. BA^+ is butylammonium; AVA^+ is ammonium valeric acid; PMA^+ is phenylmethylammonium; PEA^+ is phenylethylammonium; NMA^+ is naphthylmethylammonium. Source [30]

Two-dimensional perovskite classification

2D perovskites used in PSCs can be classified into Ruddlesden-Popper (RP) and Dion-Jacobson (DJ) as determined by the type of organic cations they possess. The general formula for RP perovskites is $R_2A_{n-1}Pb_nX_{3n+1}$ and the formula for DJ perovskites is $RA_{n-1}Pb_nX_{3n+1}$, where R is large organic spacer cation; A represents small organic cation having ability to form 3D perovskite; X is halogen (Cl, Br, I); n is the quantity of slabs. While RP 2D perovskites contain monoammonium cations that give interchanging hydrogen bonding interactions between the inorganic and organic layers, the DJ 2D perovskites contain diammonium cations (figure **1.8.**). RP 2D perovskites offer weak van der Waals interactions between these layers, contrarily, the perovskites containing diammonium cations have improved binding between the systems granting higher structural stability [32].

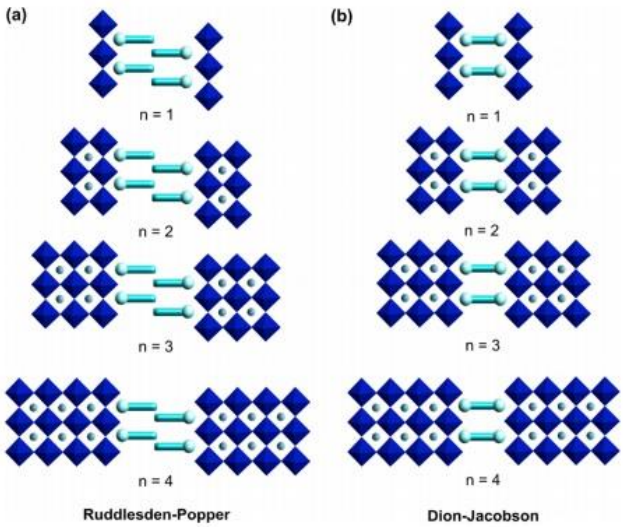

Figure 1.8. Types of two-dimensional layered perovskites whereas (a) Ruddlesden-Popper has a configuration with monovalent spacers and (b) Dion-Jacobson has a configuration with divalent spacers, as well as a distinct number of inorganic layers. Source [32]

Although, both 2D perovskite groups share similarities, yet they form slabs that fall differently on top of each other, and they have slightly different formulas. For these reasons, distinct properties are observed and their advantages and disadvantages in PSC are discussed further below.

1.3.1. Two-dimensional Ruddlesden-Popper perovskite solar cells

Structure of two-dimensional Ruddlesden-Popper perovskites

S. N. Ruddlesden and P. Popper were the first researchers to synthesize and describe a RP structure of $Sr_3Ti_2O_7$ [33]. RP phases are characterized by perovskite layers (formula of $APbX_3$) with rock-salt layers (RX). Nowadays, single, double, or triple perovskite layers are the most popular in RP phases.

RP have attracted a lot of attention as a new group of layered perovskite derivatives. Just like simple perovskites, RP 2D perovskites also have changeable oxygen stoichiometries, as well as rich chemical structure. Moreover, it is possible to change the dimensions of the layered structure and increase chemical space of RP perovskites simply by modifying the layer number n [34].

Properties of two-dimensional Ruddlesden-Popper perovskites

RP 2D perovskites can provide a great deal of opportunities for the arrangement and composition within a solar cell in terms of electronic, structural, and chemical properties. Different properties are obtained for multiple reasons: it is possible to change the numbers of the perovskite layers, also attributes of the elements in the structure (their amount, valence, particularity) and so on. RP 2D perovskites have a capability of fast charge transfer, which means they have high electrical conductivity. This factor is an advantage to many electrochemical processes. When the number of the layers grow, electronic conductivity also raises. Moreover, RP 2D perovskites display thermal and chemical stability. The structures are stable under working conditions in acidic, alkaline, and neutral solutions and even show enhanced chemical stability in elevated working conditions, which is because of rock-salt layer on the perovskite layer that provides with stabilizing effect.

Unlike basic perovskites, RP 2D perovskites can implement different physicochemical properties, all thanks to versatility in the structure. Basic perovskites also hardly have functional properties such as magnetoresistance, ferromagnetism, ferroelectricity, superconductivity, and a broad range of catalytic properties as well. Therefore, RP 2D perovskites are being used more and way more research is focused on them, compared to simple perovskites, to achieve high PCE [34, 35].

1.3.2. Two-dimensional Dion-Jacobson perovskite solar cells

DJ 2D perovskites have similar structural and optoelectronic characteristics with RP 2D perovskites. This phase is novel and only became researched by scientists recently, after RP 2D perovskites showed increased moisture stability. It is believed that DJ 2D perovskites could also display thermal and chemical stability, as well as, have properties like superconductivity, ferromagnetism and so on, but more research needs to be done in this field.

Comparison of RP 2D and DJ 2D perovskites

DJ perovskites have an advantage over RP 2D perovskites because of differences in the structure. As it is already mentioned before, RP 2D perovskites have two sheets of organic cations and these cations only interact with inorganic layers at one side, forming a van der Waals gap between adjacent organic monoammonium cations. Weak van der Waals interaction cannot guarantee moisture stability or other external strain. On the other hand, in DJ 2D perovskites diammonium cations form hydrogen bonds with inorganic layers eliminating all the gaps. They also possess higher phase purity and perovskite layers are not as distorted compared to RP 2D ones. Moreover, charge mobility is improved as well, solely by making the space between inorganic layers smaller and eliminating the gap [36, 37].

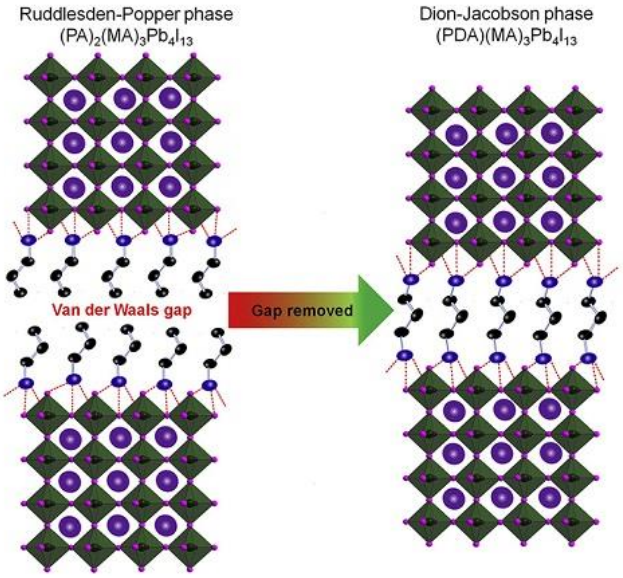

Figure 1.9. Ruddlesden-Popper compared to Dion-Jacobson and their advantage over the former, as Ruddlesden-Popper forms undesired van der Walls gap in the structure. Source [37]

S. Ahmad et al. have developed efficient and stable series of DJ 2D perovskites $(PDA)(MA)_{n-1}Pb_nI_{3n+1}$ to find out the effects of van der Waals gap and how eliminating it benefits the structure (figure **1.9.**). Findings demonstrated that DJ 2D perovskites have better efficiency and stability in PSC than RP 2D ones [37]. Therefore, DJ 2D perovskites possess similar properties to their counterparts, yet they have an advantage over RP 2D perovskites which could benefit PSC and increase stability, as well as PCE.

1.4. Three-dimensional perovskite solar cells

3D PSCs undeniably reach higher PCEs than 2D PSCs, as they could even compete with commercial silicon solar cells. 3D perovskite has the general formula of ABX_3, so it is, indeed, a simple perovskite (figure **1.10.**) [38]. Recently, the PCE of such PSCs reached up to 25.27% and a monolithic silicon/perovskite tandem skyrocketed over 29% [6, 39]. As these PSC have very high PCEs, however they have low ambiental stability that causes issues for commercial use.

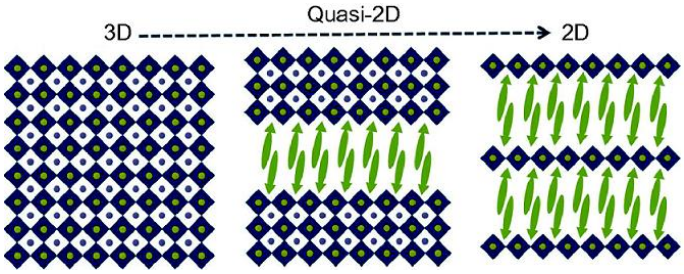

Figure 1.10. 3D and 2D RP perovskite structure comparison where inorganic layers are dark blue and organic spacers are shown as green. Source [38]

Single 3D perovskites demonstrate low moisture stability, on the other hand, 2D and quasi-2D perovskites are one of the most credible paths towards stable PSCs. Spacer cations show effective passivation of the trap states of the initial perovskite film enhancing moisture stability [40]. Therefore, mixing 2D with conventional 3D halide perovskites stability issues can be resolved. 2D/3D perovskites might hold many combined advantages, such as high PCEs from 3D perovskites and high stability from 2D perovskites with spacer organic cations.

P. Huang et al. demonstrated how PCE of 3D, RP and DJ PSCs changed in time. It was discovered that 3D holds highest PCE and even though DJ PSC were only studied after RP PSCs, their PCE caught up with the latter [41]. Moreover, X. Jiang et al. conducted an experiment under highly humid atmosphere to discover how it affects 3D, DJ 2D/3D and RP 2D/3D PSCs. After 125 hours 3D PSC has completely degraded, and after 350 hours DJ 2D/3D PSC was affected the least out of three [42]. Which means, DJ 2D/3D PSC showed better resistance to moisture than RP 2D/3D PSC (figure **1.11.**).

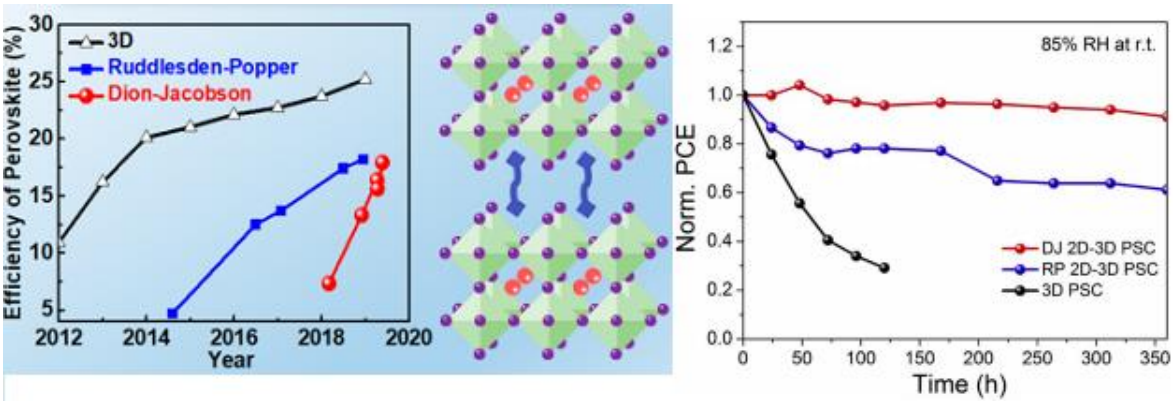

Figure 1.11. Comparison of DJ 2D/3D, RP 2D/3D and 3D perovskites. (left) PCE evolution of different perovskites; (right) stability of different perovskites at 85% relative humidity and room temperature after 350 hours. Source [41,42]

To sum up, 3D PSCs have the highest PCE, but are not stable in humid atmosphere, on the other hand DJ 2D/3D perovskites show the best resistance to moisture. The mixture of 2D/3D perovskites with DJ phases, possessing diammonium cations, have a potential to give high PCEs as well as moisture stability.

1.5. Organic cations in perovskite solar cells

Organic cations have a direct influence over the 2D perovskite thermal stability, hydrophobicity and crystallinity. It has a bigger impact in the chemical properties of the material than previously thought. For instance, simply including fluorinated cations increases tolerance to humidity. Also, a cation being monoammonium or diammonium has a great impact on PSCs efficiency and moisture stability.

C. Ma et al. reported that slimming the distance between inorganic perovskite slabs by using 1,3-propanediamine (PDA) in 2D perovskite framework could increase PCE and stability of PSCs. Hence, the charge transport was improved as well [43]. This means that using diammonium cations is more beneficial than using monoammonium organic spacers (figure **1.12.**).

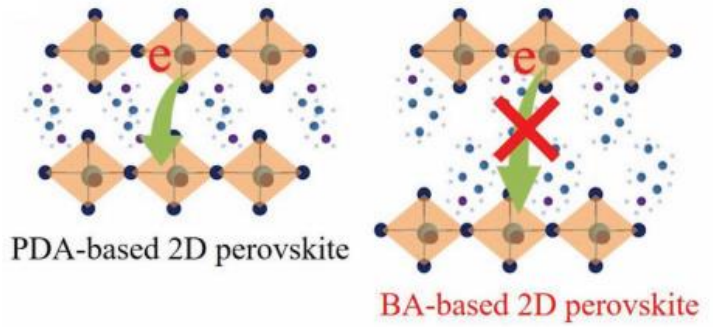

Figure 1.12. Charge transport comparison between diammonium and monoammonium cations integrated between inorganic layers, where PDA stands for propane-1,3-diammonium and BA stands for *n*-butylammonium. Source [43]

I.Garcia-Benito et al. have synthesized fluorinated aliphatic cations varying in length to form stable 2D hybrid perovskites. When exposed to humid environments and atmosphere conditions fluorinated cations are able to convey stability for 2D PSC. It was also demonstrated that the length of organic spacer highly influences PSC properties inducing a variation of the band gap and exciton binding energy, because they modulate PSC electronic structure. The shorter the organic spacer cation, the larger the band gap and that results in higher exciton binding energy and bigger effective masses, which makes shorter fluorinated cations have worse transport [44]. Moreover, adding fluorinated cations and changing the length of the molecule also influences the whole system of function, as fluorinated cations have water repellent abilities. In general, all these properties and characteristics make fluorous 2D perovskites perfect for use in stable PSCs (figure **1.13.**).

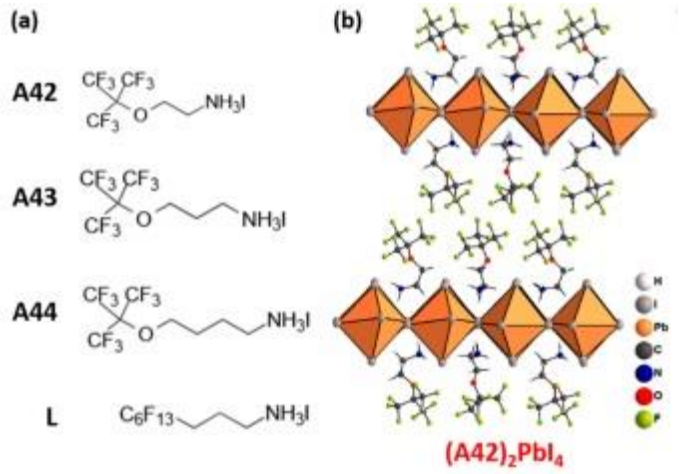

Figure 1.13. a) Molecular structure of synthesized and studied different fluorous cations, having different length; b) schematic structure of 2D hybrid perovskites with A42 as the organic spacer between the inorganic PbI_6 layers. Source [44]

D. Lu et al. have synthesized a thiophene-based diammonium iodide named ThDMAI and used in quasi-2D DJ PSCs. They compared the PCE of control device with 6.11% and ThDMAI-based device reaching 15.75%. PCE and the stability was significantly improved comparing to 3D counterparts due to the hydrophobic property of the bulky organic spacer demonstrating that DJ 2D PSCs are emerging very rapidly, assuring moisture stability and might hold potential to be used in 2D/3D PSCs (scheme **1.1.**) [45].

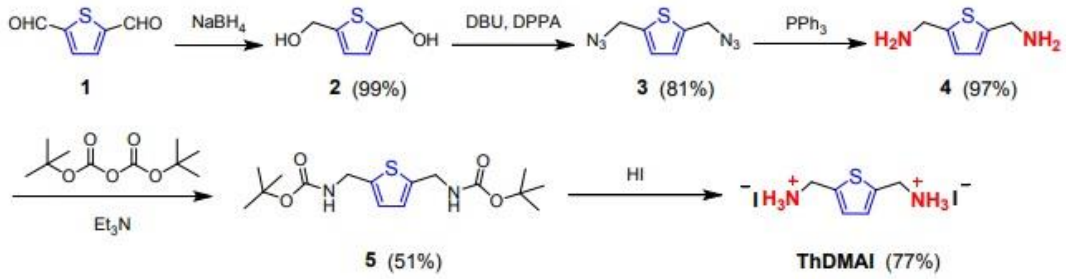

Scheme 1.1. Synthetic route of ThDMAI which have been used in 2D DJ PSC. Source [45]

The synthesis route is very similar to the conducted in this work which are described in another section. At first, the aldehyde labelled as 1 went through reduction reaction to get the compound labelled as 2. Afterwards, the hydroxyls were changed to azides and then Staundinger reaction conducted to obtain compound named as 4. In order to have pure compound ThDMAI, 4 was protected with di-*tert*-butyl dicarbonate and in the end, HI was added to obtain final product – ThDMAI.

1.6. Summary of literature review

Solar energy use is unavoidable for cheap and environmentally friendly future. Solar panels are getting better and more efficient every year, especially PSCs. PSCs efficiency skyrocketed just in a decade, therefore they hold a lot of potential. 3D perovskites have very high PCEs compared to low dimension 2D perovskites, however they have lower moisture stability and cannot be used commercially yet. 2D perovskites, on the other hand, are less efficient but they can incorporate large organic cations that increase moisture stability. Organic cations play a big role in stabilizing

PSCs and enhancing efficiency. It is noted that DJ 2D perovskites in 2D/3D structure give better moisture resistance and better PCE results than RP 2D perovskites. Moreover, fluorinated cations show water repellent properties. In conclusion, connecting 3D perovskites with 2D DJ perovskites it is hoped to obtain both advantages – very high PCE and better stability.

2. Experimental details

2.1. General methods

Nuclear magnetic resonance

^{1}H nuclear magnetic resonance (NMR) spectra were recorded at 400 MHz on a Bruker Avance III spectrometer with a 5 mm double resonance broad band BBO z-gradient room temperature probe. ^{13}C NMR spectra were collected using the same instrument at 101 MHz. The chemical shifts, expressed in ppm, were relative to tetramethylsilane (TMS). All the NMR experiments were performed at 25 °C.

Elemental analysis

Elemental analysis was performed with an Exeter Analytical CE-440 elemental analyser, Model 440 C/H/N/.

Mass spectrometry (MS)

Mass spectrometry (MS) were recorded on Waters SQ Detector 2 Spectrometer using electrospray ionization (ESI) technique.

X-ray diffraction

X-ray diffraction (XRD) patterns were measured using the Bruker D8 Advance diffractometer.

Photoluminescence measurement

The photoluminescence measurement was performed with the Flourolog-3 (Horiba Scientific) with an excitation wavelength of 450 nm.

Absorbance measurement

The absorbance spectra were obtained using a Lambda 950S (PerkinElmer, Inc.).

Current density (*J*)-voltage (*V*) measurement

Current density (*J*)-voltage (*V*) characteristics of the devices were characterized by a commercial solar simulator (Oriel, 450 W xenon, AAA class) combined with a Keithley 2400 source meter at room temperature (RT). The light intensity was calibrated before each measurement with a Si reference cell (KG5, Newport) to match with the AM 1.5G (100 mW cm^{-2}) standard. The voltage scan rate and scan step were 125 mV s^{-1} and 10 mV, respectively. No light soaking or voltage bias was applied before the measurement and the active area was 0.09 cm^2.

Stability test

The stability test was conducted under 100 mW cm^{-2} LED illumination at 25°C and the devices were sealed in a cell holder flushed with a N_2 flow of ~30 mL/min. The *J*-*V* characteristics of solar cells were traced at the maximum power point using a maximum power point tracing (MPPT) algorithm. For the humidity test, the unsealed solar cells were kept in the ambient of 30-40% relative humidity (RH) monitored by a hygrometer at room temperature in dark.

2.2. Materials

Chemicals required for the synthesis were purchased from Sigma-Aldrich and TCI Europe and used as received without additional purification. Reactions were monitored by thin-layer chromatography on ALUGRAM SIL G/UV254 plates and developed with UV light. Silica gel (grade 9385, 230–400 mesh, 60 Å, Aldrich) was used for column chromatography.

Lead iodide (PbI_2, 99.99%) and lead bromide ($PbBr_2$, 98%) were purchased from Tokyo Chemical Industry Co., LTD. Methylammonium iodide (MAI, >99.5%), cesium iodide (CsI, >99.9%), methylammonium chloride (MACl, >99.5%), formamidinium iodide (FAI, >99.5%) and Spiro-MeOTAD (>99.0%) were purchased from the Xi'an Polymer Light Technology Corp. All reagents were used as received without further purification.

2.3. Description of synthesis

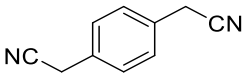

2,2'-(1,4-phenylene)diacetonitrile (1)

NaCN (1.85 g, 37.77 mmol) and 1,4-bis(bromomethyl)benzene (5.00 g, 18.94 mmol) were dissolved in EtOH (10 mL) and distilled H_2O (5 mL) and refluxed for 7 hours. After cooling to RT reaction mixture was extracted with EtOAc (3 x 100 mL), dried over anhydrous Na_2SO_4, filtered and solvent evaporated *in vacuo*. Then the product was purified by column chromatography on silica gel using 20-40% acetone in hexane. Yield 2.41 g (81%).

^{1}H NMR (400 MHz, Chloroform-*d*) δ 7.36 (s, 4H), 3.77 (s, 4H).

^{13}C NMR (101 MHz, $CDCl_3$) δ 130.48, 129.23, 117.95, 23.79.

Elemental analysis calcd (%) for $C_{10}H_8N_2$: C 76.90; H 5.16; N 17.94; found: C 76.95; H 5.32; N 17.77.

$C_{10}H_8N_2[M^+]$ exact mass = 156.07, MS (ESI) = 156.18.

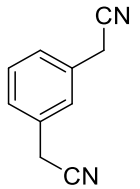

2,2'-(1,3-phenylene)diacetonitrile (2)

NaCN (2.04 g, 41.62 mmol) and 1,3-bis(bromomethyl)benzene (5.50 g, 20.83 mmol) were dissolved in EtOH (10 mL) and distilled H_2O (5 mL) and stirred for 1 hour under reflux. After that reaction mixture was extracted with EtOAc (3 x 100 mL), dried over Na_2SO_4, filtered and solvent evaporated. Then the product was purified by column chromatography on silica gel using 20% acetone in hexane. Yield 2.20 g (67%).

^{1}H NMR (400 MHz, Chloroform-*d*) δ 7.45 – 7.37 (m, 1H), 7.34 – 7.28 (m, 3H), 3.77 (s, 4H).

^{13}C NMR (101 MHz, $CDCl_3$) δ 131.42, 130.36, 128.06, 127.82, 117.72, 23.81.

Elemental analysis calcd (%) for $C_{10}H_8N_2$: C 76.90; H 5.16; N 17.96; found: C 75.78; H 5.37; N 17.65.

$C_{10}H_8N_2[M^+]$ exact mass = 156.07, MS (ESI) = 154.96.

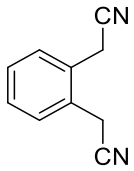

2,2'-(1,2-phenylene)diacetonitrile (3)

NaCN (1.85 g, 37.77 mmol) and 1,2-bis(bromomethyl)benzene (5.00 g, 18.94 mmol) were dissolved in EtOH (10 mL) and distilled H_2O (5 mL). After being refluxed for 3 hours, reaction mixture was extracted with EtOAc and dried over Na_2SO_4 then distilled. The product was purified by column chromatography on silica gel using 10% acetone in hexane. Yield 1.70 g (57%).

^{1}H NMR (400 MHz, Chloroform-*d*) δ 7.50 – 7.37 (m, 4H), 3.78 (s, 4H).

^{13}C NMR (101 MHz, $CDCl_3$) δ 130.23, 129.79, 128.57, 116.84, 21.95.

Elemental analysis calcd (%) for $C_{10}H_8N_2$: C 76.90; H 5.16; N 17.94; found: C 77.65; H 5.33; N 16.93.

$C_{10}H_8N_2[M^+]$ exact mass = 156.07, MS (ESI) = 154.99.

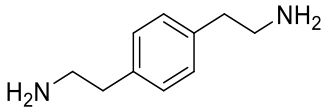

1,4-phenylenediethanamine (4)

1 (1.00 g, 6.40 mmol) was dissolved in THF (50 mL) and a solution of 1 M borane tetrahydrofuran complex (45 mL, 542.69 mmol) was added dropwise under argon atmosphere and refluxed for 24 hours. The solution was cooled down in an ice bath and THF:H_2O (v:v; 1:1) (50 mL) was added dropwise leading to a white precipitate. Then the mixture was distilled to remove THF and then EtOH (100 mL) and concentrated H_2SO_4 (1 mL) were added. Afterwards, the mixture was refluxed for 30 min. The solvents were removed *in vacuo*, 1 M NaOH (100 mL) solution was added to neutralize the acid. Next, the mixture was extracted with $CHCl_3$ (3 x 50 mL), dried over Na_2SO_4, filtered, and evaporated, leading to a white solid. The crude was used for the next step without further purification. Yield 1.05 g (99%).

$C_{10}H_{16}N_2[M^+]$ exact mass = 164.13, MS (ESI) = 164.50.

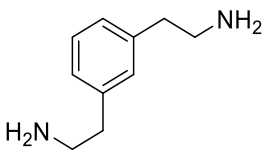

1,3-phenylenediethanamine (5)

To a solution of **2** (1.10 g, 7.04 mmol) in THF (50 mL), 1 M borane tetrahydrofuran complex solution (45 mL, 542.69 mmol) was added dropwise under argon atmosphere and refluxed for 24 hours. The reaction mixture was cooled down to RT and placed in an ice bath. THF:H_2O (v:v; 1:1) (50 mL) was added dropwise to neutralize the complex, leading to a white precipitate. Then the mixture was distilled to remove THF and EtOH (100 mL) and concentrated H_2SO_4 (1 mL) were added. Next, the mixture was refluxed for 30 min. The solvents were removed *in vacuo*, 1 M NaOH (100 mL) solution was added to neutralize the acid. And then the mixture was extracted with $CHCl_3$, dried over Na_2SO_4, filtered, and distilled, leading to a white solid. The crude was used for the next step without further purification. Yield 1.15 g (99%).

$C_{10}H_{16}N_2[M^+]$ exact mass = 164.13, MS (ESI) = 164.47.

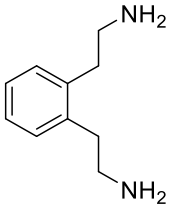

1,2-phenylenediethanamine (6)

To a solution of **3** (0.85 g, 5.44 mmol) in THF (50 mL), 1 M borane solution in THF (45 mL) was added dropwise under argon atmosphere and the mixture was refluxed for 24 hours. The solution was cooled down in an ice bath and THF:H_2O (v:v; 1:1) (50 mL) was added leading to a white precipitate. The mixture was distilled to remove THF and then EtOH (100 mL) and concentrated H_2SO_4 (1 mL) were added. Then the mixture was refluxed for 30 min. The solvents were removed *in vacuo*, 1 M NaOH (100 mL) solution was added to neutralize the acid. Next, the mixture was extracted with $CHCl_3$, dried over Na_2SO_4, filtered, and distilled, leading to a white solid. The crude was used for the next step without further purification. Yield 0.62 g (69%).

$C_{10}H_{16}N_2[M^+]$ exact mass = 164.13, MS (ESI) = 164.24.

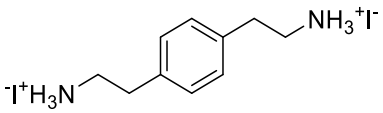

1,4-phenylenediethanaminium iodide (V1334)

4 (1.20 g, 7.30 mmol) was dissolved in CH_3OH (60 mL) and reaction flask was placed in an ice bath. HI (57 %, 12 mL) was added dropwise under argon atmosphere. Then the flask was covered with foil to avoid light exposure and stirred overnight at RT. Reaction mixture was evaporated *in vacuo* and the obtained crude was dissolved in methanol and precipitated into 20-fold excess of Et_2O. The product was filtered, washed with Et_2O and dried to yield 2.39 g of yellowish solid (77%).

^{1}H NMR (400 MHz, DMSO-d_6) δ 7.74 (s, 6H), 7.23 (s, 4H), 3.08 – 3.00 (t, J = 9.6 Hz, 4H), 2.85 – 2.81 (t, J = 9.9, 6.3 Hz, 4H).

^{13}C NMR (101 MHz, DMSO) δ 135.00, 128.26, 38.23, 31.98.

Elemental analysis calcd (%) for $C_{10}H_{18}I_2N_2$: C 28.59; H 4.32; N 6.67; I 60.42; found: C 30.02; H 4.24; N 6.4.

$C_{10}H_{18}I_2N_2[M^+]$ exact mass = 419.96, MS (ESI) = 418.82.

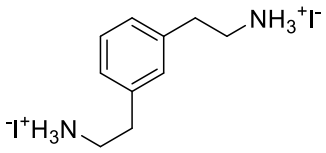

1,3-phenylenediethanaminium iodide (V1335)

5 (1.00 g, 6.08 mmol) was dissolved in CH_3OH (50 mL) under argon atmosphere. HI (57 %, 10 mL) was added dropwise while stirring the mixture in an ice bath. Afterwards, the flask was covered with foil to avoid light exposure and left to stir for 24 hours. Then the reaction mixture was evaporated *in vacuo* and the obtained crude was dissolved in methanol and precipitated into 20-fold excess of Et_2O. Precipitate was filtered, washed with Et_2O and dried to obtain the product as yellowish solid. Yield 0.62 g (23%).

^{1}H NMR (400 MHz, DMSO-d_6) δ 7.75 (s, 6H), 7.32 (t, *J* = 7.4 Hz, 1H), 7.16 (d, *J* = 8.3 Hz, 3H), 3.08 – 3.04 (t, *J* = 9.5, 6.4 Hz, 4H), 2.90 – 2.80 (t, *J* = 9.7, 6.3 Hz, 4H).

^{13}C NMR (101 MHz, DMSO) δ 137.53, 129.06, 128.96, 127.13, 38.89, 32.94.

Elemental analysis calcd (%) for $C_{10}H_{18}I_2N_2$: C 28.59; H 4.32; N 6.67; I 60.42; found: C 28.9; H 4.34; N 6.6.

$C_{10}H_{18}I_2N_2[M^+]$ exact mass = 419.96. MS (ESI) = 418.83.

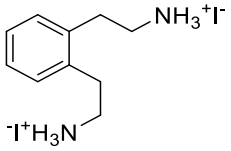

1,2-phenylenediethanaminium iodide (V1336)

6 (0.50 g, 3.04 mmol) was dissolved in CH_3OH (25 mL) and HI (57 %, 5 mL) was added dropwise under argon atmosphere while stirring the mixture in an ice bath. The flask was covered with foil to avoid light exposure and left to stir for 24 hours. After that, reaction mixture was evaporated *in vacuo* and the obtained crude dissolved in methanol and precipitated into 20-fold excess of Et_2O. Finally, precipitate was filtered, washed with Et_2O and dried to obtain the product as yellowish solid. Yield 1.00 g (78%).

^{1}H NMR (400 MHz, DMSO-d_6) δ 7.78 (s, 6H), 7.26 (s, 4H), 3.08 – 2.97 (t, 4H), 2.97 – 2.84 (t, 4H).

^{13}C NMR (101 MHz, DMSO) δ 135.50, 129.61, 129.40, 127.27, 45.39, 40.20, 38.89, 29.69.

Elemental analysis calcd (%) for $C_{10}H_{18}I_2N_2$: C 28.59; H 4.32; N 6.67; I 60.42; found: C 30,25; H 4,26; N 6,2.

$C_{10}H_{18}I_2N_2[M^+]$ exact mass = 419.96. MS (ESI) = 418.83.

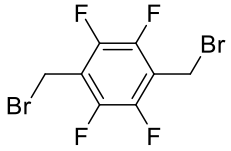

1,4-bis(bromomethyl)-2,3,5,6-tetrafluorobenzene (7)

A solution of PBr_3 (77.33 mL, 285.71 mmol, 6 eq) in CH_2Cl_2 (38 mL) was added dropwise during 1 hour to a solution of (perfluoro-1,4-phenylene)dimethanol (10.00 g, 47.61 mmol) in DMF (94 mL) at 0°C under argon atmosphere. Resulting solution was stirred at RT for 3 hours and then treated with H_2O (200 mL) and extracted with EtOAc (3 x 200 mL). Then the solution was dried over anhydrous Na_2SO_4 and filtered. The solvent was evaporated *in vacuo* and the residue was chromatographed on silica gel using hexane to acquire **1** as white powder. Yield 14.59 g (91%).

^{1}H NMR (400 MHz, $CDCl_3$) δ 4.51 (s, 4H).

^{13}C NMR (101 MHz, $CDCl_3$) δ 146.00, 143.41, 117.70, 16.35.

Elemental analysis calcd (%) for $C_8H_4Br_2F_4$: C 28.60; H 1.20; Br 47.57; F 22.62; found: C 29.39; H 1.16.

$C_8H_4Br_2F_4[M^+]$ exact mass = 335.86, MS (ESI) = 335.96.

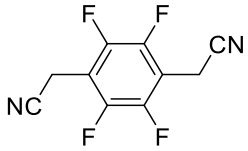

2,2'-(perfluoro-1,4-phenylene)diacetonitrile (8)

TFA (0.68 mL, 1.01 g, 8.93 mmol) was added dropwise to a stirred suspension of NaCN (0.65 g, 13.39 mmol) in dry DMSO (30 mL) at 12°C under argon atmosphere. The mixture was allowed to stir in RT for 30 min which resulted in a homogenous solution. Then a separate solution of **1** (1.5 g, 4.46 mmol) in DMSO (10 mL) was added dropwise to the TFA/NaCN mixture over 30 min while the temperature was kept at 15-18°C by external cooling. After the addition was complete the mixture was warmed to RT and stirred for 1 hour following with stirring overnight at 40°C. Reaction mixture was treated with ice-H_2O (100 mL) and the resulting suspension was extracted with EtOAc (3 x 50 mL). Combined organic extracts were dried over anhydrous Na_2SO_4 and filtered, the solvent was evaporated *in vacuo* and the crude product was chromatographed on silica gel using 10-15% acetone in hexane to give **8**. Yield 0.28 g (27%).

^{1}H NMR (400 MHz, $CDCl_3$) δ 3.83 (s, 4H).

^{13}C NMR (101 MHz, $CDCl_3$) δ 143.32, 113.87, 110.19, 30.75, 11.41.

Elemental analysis (%) calcd for $C_{10}H_4F_4N_2$: C 52.65; H 1.77; F 33.31; N 12.28; found: C 52.45; H 1.49; N 12.02.

$C_8H_4F_4N_2[M^+]$ exact mass = 228.03, MS (ESI) = 228.59.

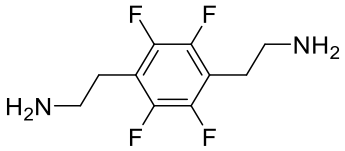

2,2'-(perfluoro-1,4-phenylene)bis(ethan-1-amine) (9)

8 (0.28 g, 1.22 mmol) was dissolved in THF (15 mL) and a solution of 1 M borane tetrahydrofuran complex (12.6 mL) was added dropwise under argon atmosphere and refluxed for 24 hours. Then the solution was cooled down in an ice bath and THF:H_2O (v:v; 1:1) (15 mL) was added dropwise and then the mixture was distilled to remove THF. Afterwards, EtOH (60 mL) and concentrated H_2SO_4 (0.5 mL) were added. The mixture was refluxed for 30 min. Next, the solvents were removed *in vacuo*, 1 M NaOH (100 mL) solution was added to neutralize the acid. The mixture was extracted with $CHCl_3$ (3 x 50 mL), dried over Na_2SO_4, filtered, and evaporated. The crude was used for the next step without further purification. Yield 0.27 g (93%).

$C_{10}H_{12}F_4N_2[M^+]$ exact mass = 236.09, MS (ESI) = 236.48.

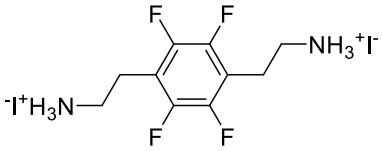

2,2'-(perfluoro-1,4-phenylene)bis(ethan-1-aminium) iodide (V1402)

9 (0.25 g, 1.05 mmol) was dissolved in CH_3OH:THF (v:v; 1:1) (40 mL) and reaction flask was placed in an ice bath. HI (57 %, 0.30 mL, 2.32 mmol, 2.2 eq) was added dropwise under argon atmosphere. The flask was covered with foil to avoid light exposure and stirred for 24 hours at RT. After that, reaction mixture was evaporated *in vacuo* and the obtained crude was dissolved in methanol and precipitated into 20-fold excess of Et_2O. Finally, the product was filtered, washed with Et_2O and dried to yield 0.30 g of yellowish solid (58%).

^{1}H NMR (400 MHz, DMSO) δ 7.87 (s, 6H), 3.02 (s, 8H).

^{13}C NMR (101 MHz, DMSO) δ 145.76, 143.37, 114.36, 40.15, 37.63, 20.64.

Elemental analysis calcd (%) for $C_{10}H_{14}F_4I_2N_2$: C 24.41; H 2.87; F 15.44; I 51.58; N 5.69; found: C 25.30; H 2.78; N 5.79.

$C_{10}H_{14}F_4I_2N_2[M^+]$ exact mass = 491.92, MS (ESI) = 491.18.

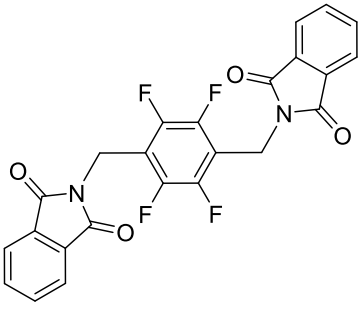

2,2'-((perfluoro-1,4-phenylene)bis(methylene))bis(isoindoline-1,3-dione) (10a)

Potassium phthalimide (5.43 g, 29.76 mmol, 4 eq) was added to a solution of **7** (2.50 g, 7.44 mmol) in DMF (250 mL) and stirred at 100°C overnight. Then the mixture was cooled down to RT and poured into H_2O (100 mL), and precipitate filtrated to afford 2.76 g of **10a** as white solid (79%).

^{1}H NMR (400 MHz, $CDCl_3$) δ 7.91 – 7.63 (m, 8H), 4.96 (s, 4H).

^{13}C NMR (101 MHz, $CDCl_3$) δ 167.24, 143.91, 143.80, 134.39, 131.93, 123.70, 30.18, 30.15.

Elemental analysis calcd (%) for $C_{24}H_{12}F_4N_2O_4$: C 61.55; H 2.58; F 16.23; N 5.98; O 13.66; found: C 61.41; H 2.63; N 5.98.

$C_{24}H_{12}F_4N_2O_4[M^+]$ exact mass = 468.07, MS (ESI) = 468.55.

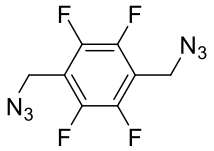

1,4-bis(azidomethyl)-2,3,5,6-tetrafluorobenzene (10b)

To a solution of **7** (3.50 g, 10.41 mmol) in $(CH_3)_2CO$ (40 mL) was added NaN_3 (3.58 g, 55.22 mmol, 5.3 eq) and refluxed for 2 hours. The resulting solution was extracted with $(C_2H_5)_2O$ (3 x 100 mL) then dried over anhydrous Na_2SO_4 and filtered. Finally, the solvent was evaporated *in vacuo* to give **10b**. Yield 2.40 g (89 %).

^{1}H NMR (400 MHz, $CDCl_3$) δ 4.49 (s, 4H).

^{13}C NMR (101 MHz, $CDCl_3$) δ 146.30, 143.85, 115.21, 77.48, 77.16, 76.84, 42.07, 0.13.

Elemental analysis calcd (%) for $C_8H_4F_4N_6$: C 36.93; H 1.55; F 29.21; N 32.30; found: C 32.87; H 1.38; N 23.85.

$C_8H_4F_4N_6[M^+]$ exact mass = 260.04, MS (ESI) = 260.90.

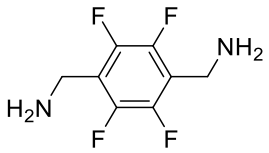

(perfluoro-1,4-phenylene)dimethanamine (11)

10a (1.5 g, 3.20 mmol) was dissolved in THF:ethanol (v:v; 1:1) (100 mL) and $N_2H_4 \cdot H_2O$ (64%, 0.6 mL, 3 eq) was added dropwise into the solution. The mixture was refluxed for 3 hours, and the formed precipitate filtrated, washed with ethanol (100 mL) and the filtrate was distilled to obtain a solid product. Yield 0.09 g (13 %).

$C_8H_8F_4N_2[M^+]$ exact mass = 208.06, MS (ESI) = 208.88.

10b (2.00 g, 7.69 mmol) was dissolved in THF (15 mL) and added dropwise into the solution of $LiAlH_4$ (95%, 0.68 g, 2.23 eq) in THF (10 mL) at 0°C under argon atmosphere. Then the mixture was stirred at RT for 1 hour and 1M NaOH (50 mL) solution was added. H_2O (100 mL) was added

dropwise, and the formed precipitate was filtrated. Filtrate was extracted with CH_2Cl_2 (3 x 50 mL), dried over anhydrous Na_2SO_4 and evaporated in vacuo to obtain a product. Yield 0.52 g (32 %).

$C_8H_8F_4N_2[M^+]$ exact mass = 208.06, MS (ESI) = 208.88.

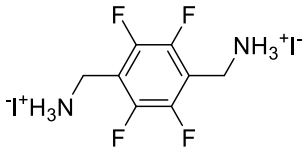

(perfluoro-1,4-phenylene)dimethanaminium iodide (V1372)

11 (0.52 g, 2.49 mmol) was dissolved in THF (50 mL) and reaction flask was placed in an ice bath. HI (57 %, 0.72 mL, 2.2 eq) was added dropwise under argon atmosphere. The flask was covered with foil to avoid light exposure and stirred for 24 hours at RT. Afterwards, reaction mixture was distilled, and the obtained crude was dissolved in CH_3OH and precipitated into 20-fold excess of Et_2O. The product was filtered, washed with Et_2O and $(CH_3)_2CO$ and dried to yield 0.95 g of yellowish solid (82 %).

^{1}H NMR (400 MHz, DMSO) δ 8.33 (s, 6H), 4.23 (s, 4H).

^{13}C NMR (101 MHz, DMSO) δ 206.52, 145.75, 143.27, 113.84, 30.72, 30.44.

Elemental analysis calcd (%) for $C_8H_{10}F_4I_2N_2$: C 20.71; H 2.17; F 16.38; I 54.70; N 6.04; found: C 19.33; H 1.86; N 5.25.

$C_8H_{10}F_4I_2N_2[M^+]$ exact mass = 463.88, MS (ESI) = 463.14.

2.4. Device fabrication

The TiO_2 compact ($cTiO_2$) layer was deposited onto the cleaned FTO (Nippon Sheet Glass, TEC8) substrates by spray pyrolysis of titanium diisopropoxide bis(acetylacetonate) (75 wt. % in isopropanol, Sigma-Aldrich) diluted in anhydrous isopropanol (99.8%, Acros Organics) with 1:20 volume ratio at 450 °C. The substrates were then annealed at 450 °C for 30 min. TiO_2 paste (30NR-D, GreatCell Solar) was diluted in anhydrous ethanol (99.8%, Acros Organics) with a weight ratio of 1:10 and spin-coated onto the $cTiO_2$ layer at 3000 rpm for 20 s. The films were then annealed at 500 °C for 30 min in air. After cooling, 0.1 M $SnCl_4$ (99%, Acros Organics) aqueous solution was deposited on the substrate at 3000 rpm for 30 s. The films were then dried at 190 °C for 1 h and transferred into a nitrogen glovebox. 1.45 M perovskite precursors (PbI_2:$PbBr_2$:FAI:MAI:CsI:MACl = 0.98:0.02:0.81:0.04:0.05:0.20) were dissolved in the mixed DMF (99.8%, Acros Organics): DMSO (99.7%, Acros Organics) = 4:1 (volume ratio) solvent. The perovskite solution was spin-coated on the substrates at 1000 rpm for 12 s and 5000 rpm for 28 s, respectively. 200 μL of chlorobenzene (99.8%, Acros Organics) was dropped onto the spinning films at 15 s before the end of the second step, followed by annealing at 100 °C for 10 min and 150 °C for 10 min. For the post treatment, organic cation solutions with a concentration of 2 mg mL^{-1} in anhydrous isopropanol (99.8%, Acros Organics) were deposited on the perovskite films at 4000 rpm for 20s, followed by annealing at 100 for 5 min. 0.06 M Spiro-OMeTAD was dissolved in chlorobenzene (99.8%, Acros Organics), with the addition of 0.2 M 4-*tert*-Butylpyridine (98%, Sigma-Aldrich), 0.03 M bis(trifluoromethanesulfonyl)-imide lithium salt (LiTFSI, 99.0%, Sigma-

Aldrich) in acetonitrile (99.9%, Acros Organics) and 0.0035 M FK209 Co(III) TFSI salt (GreatCell Solar) in acetonitrile (99.9%, Acros Organics). The Spiro-OMeTAD solution was spin-coated at 3000 rpm for 20 s, followed by the thermal evaporation of a 70 nm gold electrode under high vacuum.

3. Results and discussion

PSCs gained so much attention recently because PCE is getting higher way faster than any other earlier generation solar cell and soon it is expected to surpass them. First generation solar cells with multicrystalline silicon generally have high efficiency and can be used commercially, yet their cost is high as well. In general, second generation solar cells cost less than the first generation ones, but their efficiency is low. PSCs have a potential to change that, because cheap materials are used and they are solution-processable. However, there is an issue they have to face – degradation in humid environment faster than expected. Solar cells have regulations which they have to fit in to be available for the market. Therefore, if a solar cell cannot last and maintain its efficiency after a certain time in an ambiental environment then it irrefutably cannot be ready for commercial use. Nowadays, a typical hybrid lead halide PSC has PCE around 17-22% and the record is over 25% [6] being incredible result having in mind that theoretical PCE can reach around 30% [8]. It is hardly possible for a solar cell to surpass that line, because sun's rays are reflected, or the energy can turn to heat. In the future, other approach would have to be taken, such as a capability for a photon to excite multiple electrons at the same time in order to improve the PCE further [46].

For a perovskite to surpass the most efficient solar cells and also maintain stability would be incredible improvement overall, since PSCs have easy fabrication processes, don't cost much, and they are also lightweight. Like it was mentioned before, 3D perovskites are simple perovskites that have high PCE but their PCE gets very low in a short time when put in humid environment. On the other hand, 2D perovskites have low PCEs, but sustain in humid environments and they can also contain different organic cations in their structure that enables a variety of possible functionalization. Unlikely, 3D perovskites are limited due to the size of the organic cations in their structure. Therefore, by combining 2D/3D perovskites together it is hoped to have tunable properties – high efficiency and high stability. The most common organic cations used in 2D perovskites were named RP, containing monoammonium group. They were discovered relatively recently, in 2014 [27], and after around 4 years the new phase emerged called DJ 2D perovskites that showed improved properties. From 2014 until now, there were multiple articles in the literature written about RP 2D perovskites and how they might improve moisture resistance in perovskite solar cells. Different organic spacer cations were synthesized as well, and their properties discussed to show increased PCE and stability [47]. Only recently, it was noticed that DJ 2D perovskites can make an even bigger impact and a few articles were published on synthesized cations. However, this is a very fresh topic – experiments on 2D DJ are very scarce and it is still unknown how different cation could possibly change PCE and how much it could improve moisture stability. For this reason, in this work different 2D DJ perovskite organic spacer cations were being synthesized to figure out their prospects in 2D/3D PSC.

To date, PEAI having ethylammonium iodide group attached to the phenyl ring was found to show the highest performance in RP 2D/3D PSC, while other reports have also support the idea that ethenyl spacer between the aromatic part and ammonium active site is necessary to obtain the effective formation of 2D phase [48]. Moreover, fluorinated cations are known to have water repellent properties, for this reason a strategy to insert fluorine atoms in benzene ring is employed [49]. In this work, first of all, isomeric cations having two ethylammonium iodide groups in different benzene positions are synthesised and their performance in PSC is compared. Second, fluorine atoms are inserted into the structure of *p*-phenylenediethanamonium iodide cation to find

out if moisture stability is improved. After that, ethylammonium iodide group attached to perfluorobenzene ring is shortened to methylammonium iodide having further structural comparison.

All synthesis were conducted in Kaunas University of Technology (KTU) in research group of prof. dr. V. Getautis to gain 5 distinct final products as organic spacer cations. Afterwards, the products were sent to École polytechnique fédérale de Lausanne (EPFL) in Switzerland, Group for Functional Materials headed by prof. dr. M. K. Nazeeruddin for further analysis in 2D/3D PSCs. Received results are discussed and their importance is debated below in this work.

3.1. Synthesis of diammonium cations with substituents in *ortho*-, *meta*- and *para*-positions

A multistage synthesis was performed in order to synthesize three distinct cations with ethylammonium iodide substituents in ortho, meta and para positions in benzene ring (scheme **3.1**).

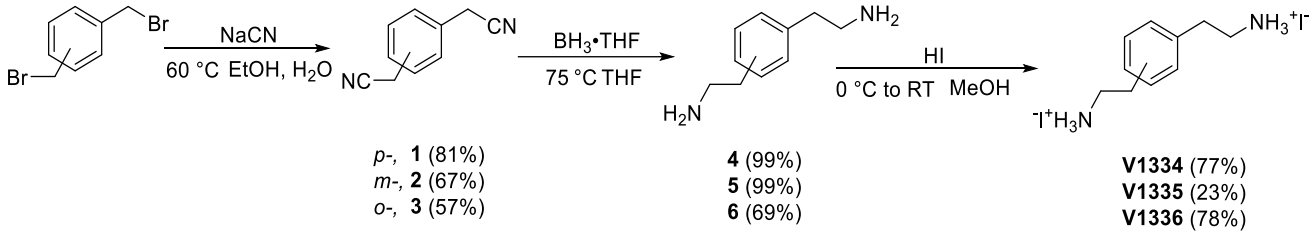

Scheme 3.1. Synthesis of 1,4-phenylenediethanaminium iodide (V1334), 1,3-phenylenediethanaminium iodide (V1335) and 1,2-phenylenediethanaminium iodide (V1336).

In the first step, the substitution reaction was carried out by substituting bromide species with cyanides using NaCN in EtOH/H_2O. Refluxing for 7 hours yielded (**1**) in 81% conversion. Similarly, substitution reactions were conducted with structures in *meta*- and *ortho*-positions with shorter reaction times of 1 and 3 hours, and lower yields of 67% and 57%, for (**2**) and (**3**), respectively.

Next, the reduction reaction was carried out to reduce the cyano groups up to the primary amines forming the precursors for active ammonium sites and elongating the aliphatic fragments in the molecule. **1-3** were dissolved in THF and the solution of borane tetrahydrofuran complex as reduction agent was introduced under argon atmosphere [50]. Obtained crude products **4-6** were used for further step without purification due to the instability and only MS spectra were recorded to verify the structures.

The final desired products 1,4-phenylenediethanaminium iodide **(V1334)**, 1,3-phenylenediethanaminium iodide **(V1335)** and 1,2-phenylenediethanaminium iodide **(V1336)** were acquired by addition reaction using HI. First, **4** was dissolved in CH_3OH and reaction flask was placed in an ice bath, HI was added dropwise under argon atmosphere at 0°C, the flask was covered with foil to avoid light exposure and stirred overnight at RT to obtain the yield of 77%. Later, **V1335** and **V1336** followed the same procedure with addition of HI, where **5** was used to acquire **V1335** (yield of 23%) and **6** was used to get **V1336** (yield of 78%).

The intermediate and final products were identified with ^{1}H (figure **3.1.**, figure **3.2.**, figure **3.3.**), ^{13}C NMR spectra, elemental analysis and MS, unless otherwise noted. All three final products were in a

form of yellow solid. After the successful synthesis, **V1334**, **V1335** and **V1336** were shipped to EPFL to be tested further for the use in PSC.

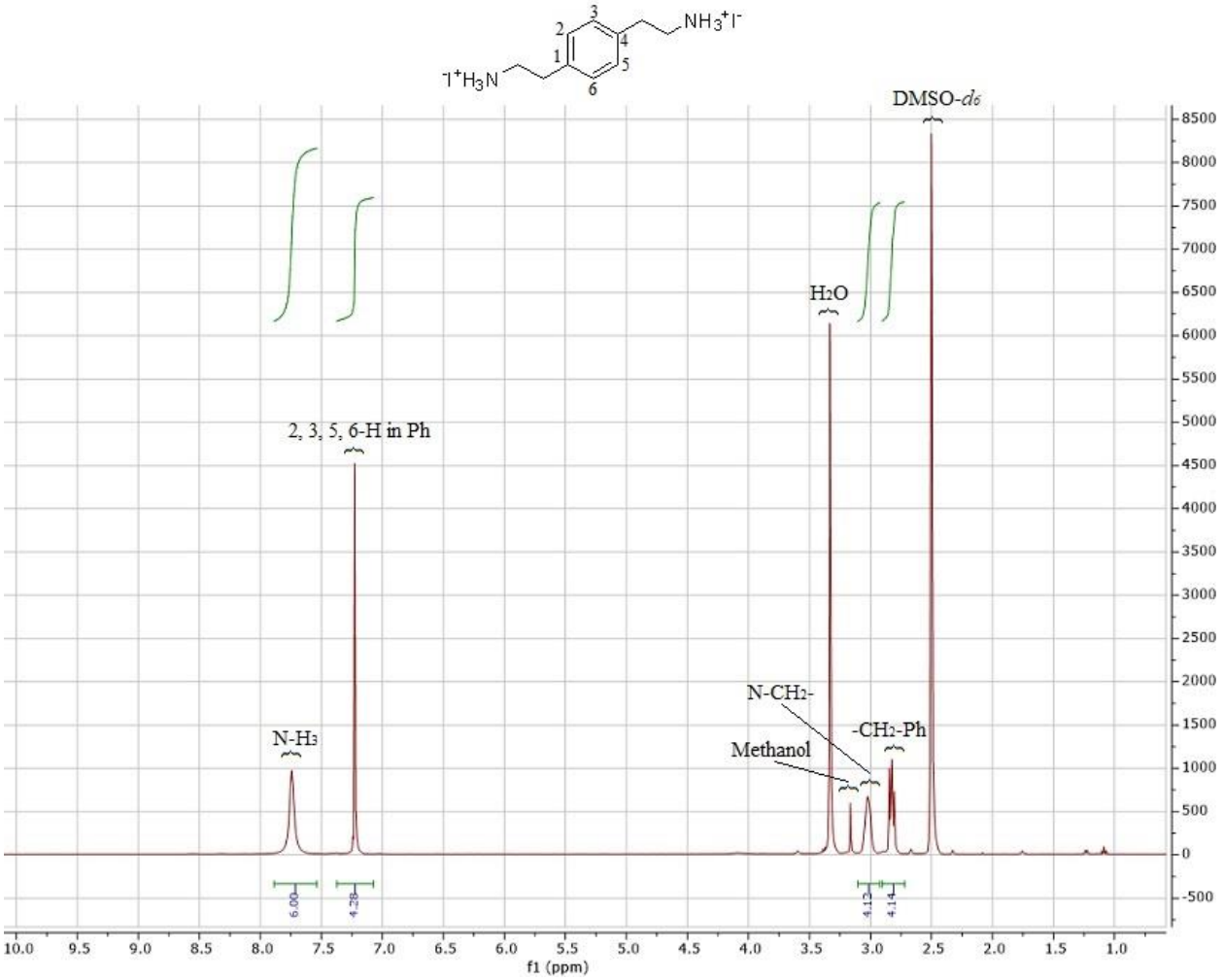

Figure 3.1. ^{1}H NMR spectrum of 1,4-phenylenediethanaminium iodide (V1334).

At 7.74 ppm protons from NH_3 groups in the molecule are observed in a singlet. Since the molecule is symmetrical, the protons from 2, 3, 5 and 6 positions in the benzene ring can be seen at 7.23 ppm in a singlet as well. The protons in the ethenyl linkers can be detected from 3.08 to 2.81 ppm, where N-CH_2- is observed at 3.08 – 3.00 in a triplet and -CH_2-Ph group's protons are fixated at 2.85 – 2.81 in a triplet also. The spectrum has side solvents such as DMSO-d_6 at 2.50 ppm, methanol at 3.16 ppm and H_2O at 3.33 ppm.

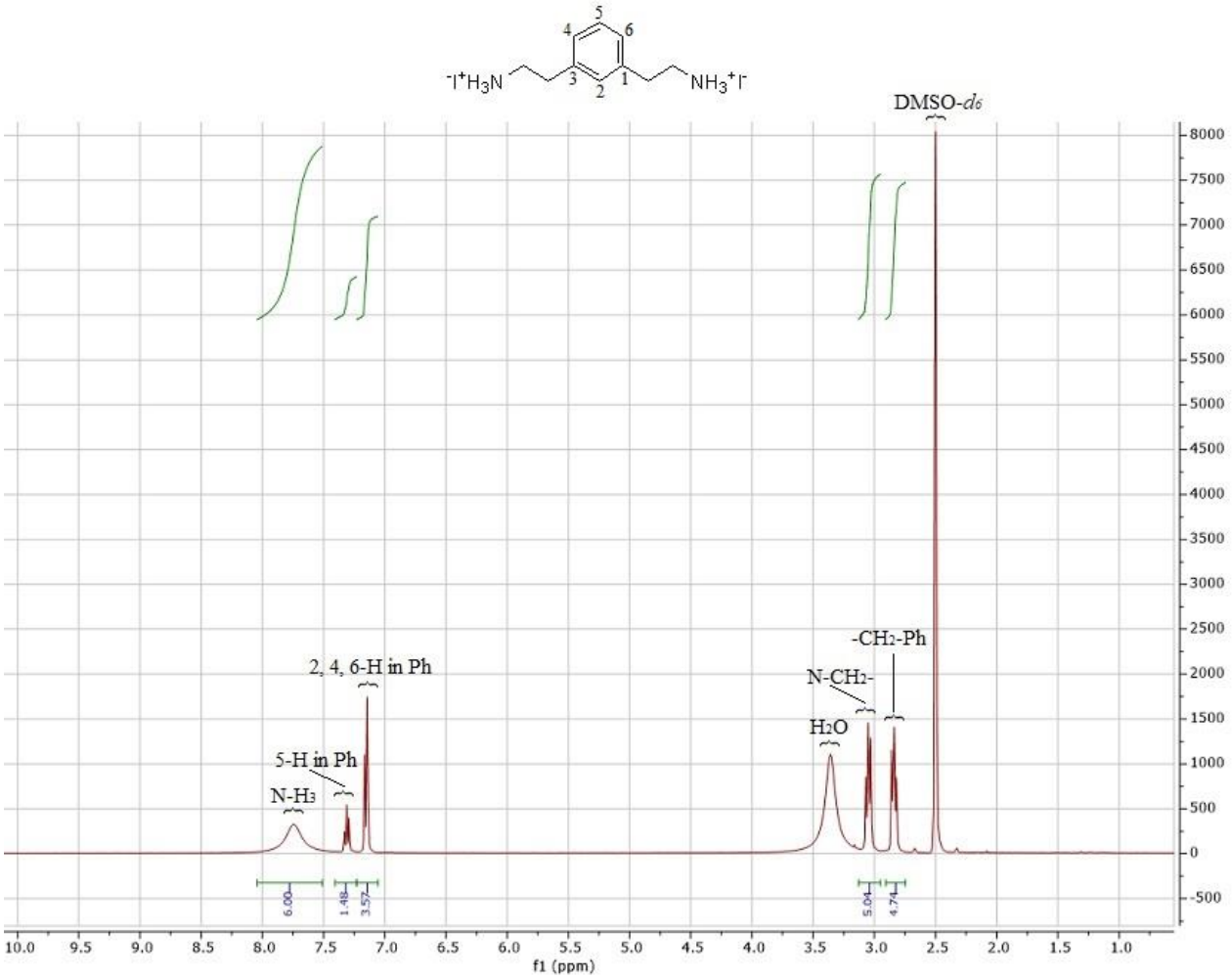

Figure 3.2. ^{1}H NMR spectrum of 1,3-phenylenediethanaminium iodide (V1335).

In the spectrum of **V1335** NH_3 protons are observed at 7.75 ppm. This molecule has ethenyl linkers in *meta*-position for this reason different signals of protons in benzene ring are observed separately. Proton in the benzene ring, which carbon atom does not connect to any other carbon atom that has ethenyl groups, has a triplet at 7.32 ppm. Protons in positions of 2, 4 and 6 in the benzene ring (where 1 and 3 is where ethenyl linkers are) show a duplet at 7.16 ppm. At 3.08 – 3.04 a triplet from N-CH_2- group is observed. Then, at 2.90 – 2.80 a triplet from -CH_2-Ph can be seen. DMSO-*d_6* is fixated at 2.50 ppm and H_2O at 3.33 ppm.

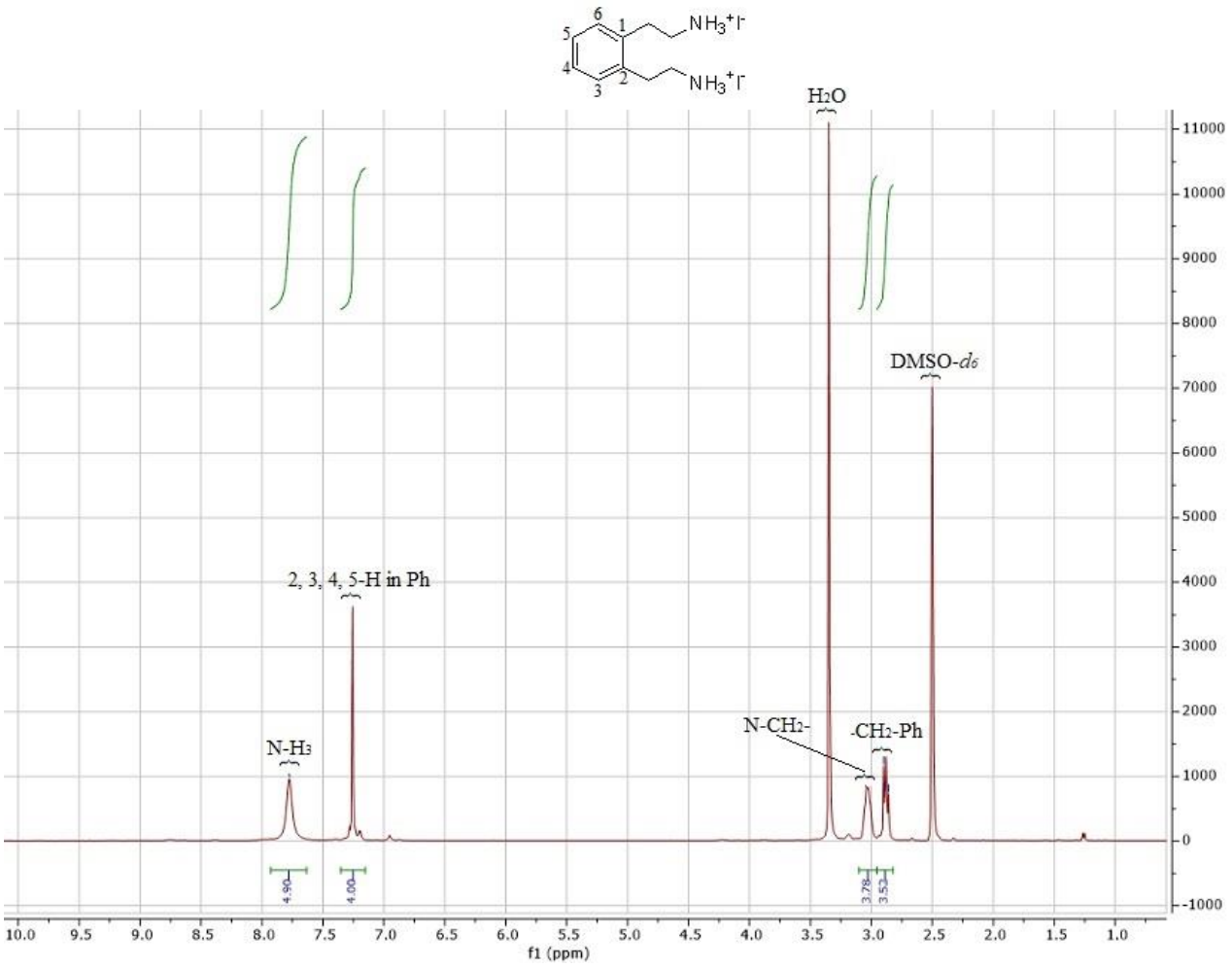

Figure 3.3. ^{1}H NMR spectrum of 1,2-phenylenediethanaminium iodide (V1336).

In this spectrum, where ethenyl groups are placed close to each other (*ortho*- position in the ring) a singlet at 7.78 ppm from NH_3 protons is observed. At 7.26 ppm a singlet is observed from all the other left protons in the benzene ring (in 2, 3, 4 and 5 positions). Then, at 3.08 – 2.97 ppm N-CH_2- groups are seen in a triplet, where -CH_2-Ph is at 2.97 – 2.84 as a triplet as well. DMSO-d_6 is detected at 2.50 ppm and H_2O at 3.33 ppm.

Spectra of all three **V1334**, **V1335** and **V1336** are quite similar, the biggest difference is observed in 7.28 – 7.16 ppm region, because in this site the protons in the benzene ring interact differently with ethenyl groups attached. **V1334** and **V1336** both have a singlet at 7.74 ppm and 7.78 ppm respectively, where **V1335** shows a singlet, a triplet and a duplet. N-CH_2- groups are detected in 3.08 – 2.97 region and -CH_2-Ph at 2.97 – 2.81 ppm region overall.

3.1.1. Effieciency and stability of diammonium cations with substituents in *ortho*-, *meta*- and *para*-positions

Synthesized organic spacer cations **V1334**, **V1335** and **V1336** were further used for the 2D perovskite formation. Different analytical methods were applied to find out if cations having the active ammonium sites in isomeric positions may form the 2D perovskite phase. Typically, 2D phase is made upon mixing the precursor solution with the PbI_2 and preparing the thin-films by spin-coating and annealing them at 100 °C for several minutes.

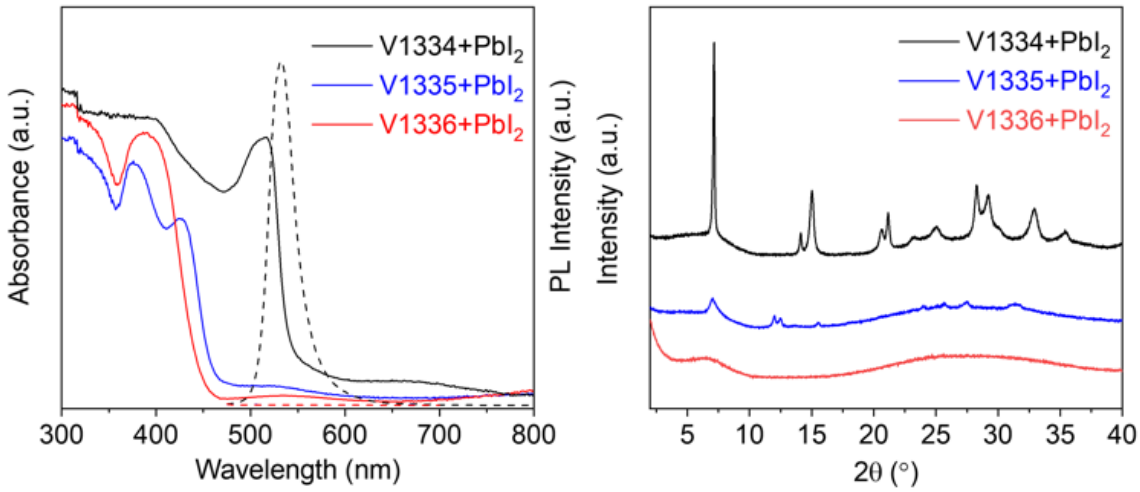

Figure 3.4. UV-Vis absorption and photoluminescence spectra of thin films of incorporated synthesized cations upon mixing with PbI_2 (left); XRD spectrum of thin films of incorporated synthesized cations upon mixing with PbI_2 (right).

As seen from figure **3.4.**, only **V1334** was able to form 2D perovskite phase, exhibiting a broad absorption with a maximum peak value between 470-550 nm, while **V1335** and **V1336** do not exhibit such peak and only bare cation absorption is detected around 400 nm. Furthermore, **V1334**-based perovskite also has a bathochromically shifted absorption and photoluminescence peak at 540 nm, while **V1335** and **V1336** showed no detectable emission. In addition, to support these findings, the same films were characterized by XRD analysis. **V1334**-based film shows a characteristic diffraction peak at 5.80°. Also, there are peaks at 15.00°, 21.00°, 28.50° and 32.00° which are typical for formed 2D perovskites. However, those peaks are only observed with integrated **V1334** cation and are nearly absent in the samples with **V1335** and **V1336**. which means that cations **V1335** and **V1336** did not form a 2D structure. Considering these results, only **V1334** could be used for formation of 2D perovskite with PbI_2 and will be used further, while **V1335** and **V1336** are not able to coordinate to the Pb most probably due to the steric hinderance.

Since only **V1334** was able to react with PbI_2 forming a functional 2D phase, it was used further for construction of quasi-2D perovskite solar cells within the architecture shown in **Figure 3.5.** Device based on a perovskite composition of (**V1334**)$MA_{(n-1)}Pb_nI_{3n+1}$, where n=9, was used and PCE of such device was tested properly with reversed and forward scan (table **3.1**.), showing 13.54% and 12.32%, respectively, which is comparable with the results described in some literature of 2D DJ phase analogues having 13.3% [51]. Having these results in mind, it is obvious that **V1334** is suitable to be used in PSC and to obtain better results further optimization is needed.

Table 3.1. Photovoltaic characteristics of V1334-based PSC.

V_{OC} (V)	J_{SC}(mA cm^{-2})	FF	PCE (%)	Composition
1.006	19.17	0.710	13.54	V1334 n=9 Reverse
982.402	19.00	0.667	12.32	V1334 n=9 Forward

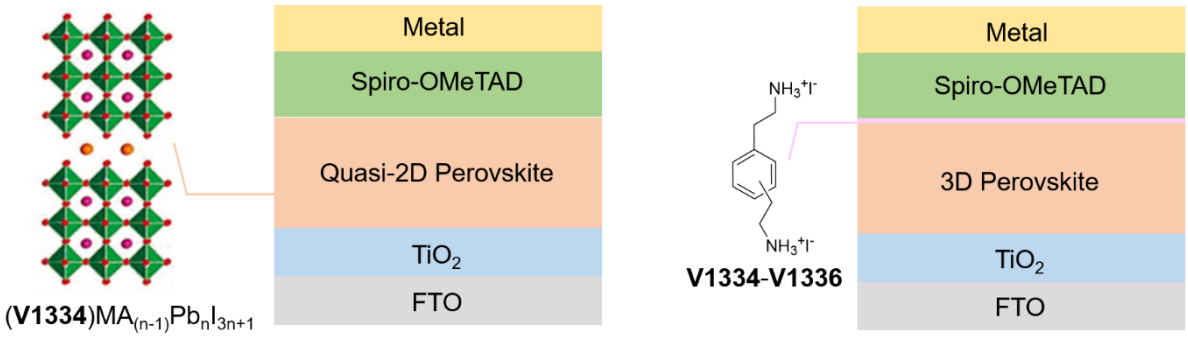

Figure 3.5. Device architectures used in this study. V1334-based quasi-2D architecture (left) and V1334-V1336 passivation layered architecture.

Due to the fact that only **V1334** cation was incorporated into the quasi-2D PSC, a different approach to use synthesised cations was considered. Gaining the advantage that all synthesised cations have free ammonium groups that could coordinate with uncoordinated Pb or passivate the crystal defects of the 3D perovskite layer, an extra passivating layer on top of 3D perovskite was spin-coated during the construction of the device as shown in the figure **3.5.** and compared to the control device having no extra passivation as the reference. Table **3.2.** summarizes the photovoltaic parameters obtained in this study. The control PSC when affected by solar simulator had PCE of 20.88±0.60 %, afterwards devices passivated with **V1334**, **V1335** and **V1336** were analysed. PSC of the device with **V1334** has not showed much difference, only slight decrease having PCE of 20.30±0.60 % was observed. However, it was observed that PSC with **V1335** had a significant decrease to reach PCE of 9.98±3.14 %. On the other hand, PSC with **V1336** showed significantly increased performance of 22.41±0.56 % PCE, demonstrating that the strategy of having an extra passivation layer on top of 3D perovskite could lead to the improved device performance. To summarize, a cation with a substitution in *ortho*-position improves the efficiency, most probably due to the beneficial arrangement of active ammonium sites in the composition.

Table 3.2. PSC passivation with different cations (V1334, V1335 and V1336) and control as the reference.

Composition	V_{oc} (V)	J_{sc}(mA cm^{-2})	FF	PCE (%)
Control	1.114±0.01	24.26±0.25	0.773±0.02	20.88±0.60
V1334	1.097±0.03	24.20±0.32	0.765±0.02	20.30±0.60
V1335	0.757±0.23	23.71±1.09	0.509±0.09	9.98±3.14
V1336	1.141±0.01	24.52±0.31	0.801±0.01	22.41±0.56

Since PSC passivated with synthesized **V1336** showed increased PCE, it was investigated more thorough. PSCs using **V1336** was tested with the control PSC which had no organic cations were tested further and their PCE was evaluated in forward and reverse scans (table **3.3.,** figure **3.6.**).

Table 3.3. PSC with V1336 and control PSC without organic spacer cations compared in reverse and forward scans.

Composition	V_{OC} (V)	J_{SC}(mA cm^{-2})	FF	PCE (%)
Control-Reverse	1.135	24.49	0.790	21.94
Control-Forward	1.107	24.22	0.758	20.32
V1336-Reserve	1.154	24.70	0.809	23.07
V1336 Forward	1.143	24.74	0.799	22.50

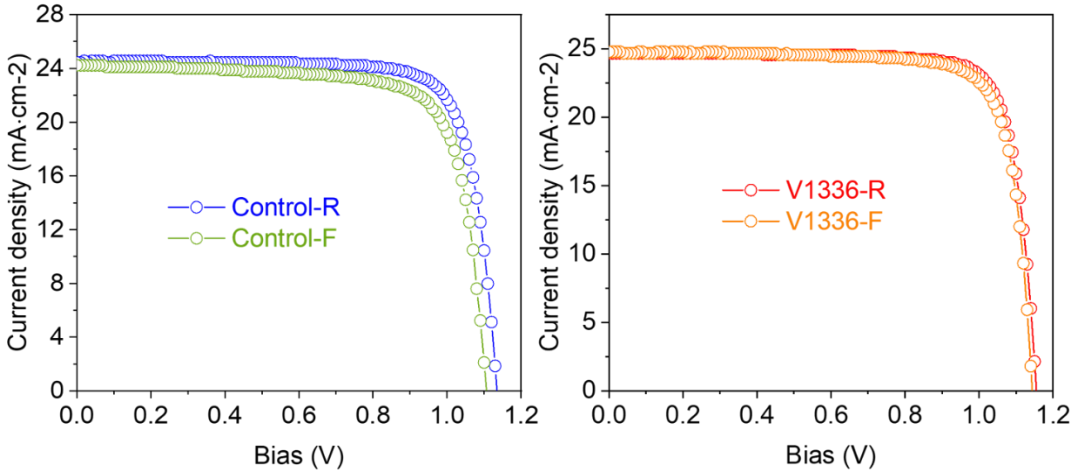

Figure 3.6. *J-V* curves and hysteresis behaviour of the perovskite solar cells containing control and V1336. Curves were measured under 1 sun intensity illumination, scanned from open-circuit to short-circuit (forward) followed by a scan from short-circuit to open-circuit (reverse) conditions, with a scan rate of 50 mV s^{-1}.

Control device shown the PCE of 20.32% in forward scan and 21.94% in reverse, respectively. It can be noted that the hysteric behaviour for a control device is quite high, while the **V1336**-passivated device had much improved performance of 23.07% in reverse scan and slightly lower PCE of 22.50% in forward scan, respectively. The smaller deviation of performance using the passivation layer of **V1336** could be explained that the passivation improves the charge transport. It also has to be noted that the PCE of 23.07% is a superior result and shows great prospects for the further optimization of passivation studies.

Same devices were further analysed in moisture stability test. Control and **V1336**-passivated PSCs were held in the environment of 40-50% relative humidity in the dark for 1000 h with the PCE being evaluated periodically. The tendency that the passivated device has improved stability over the control device could be seen in the figure **3.7.** At the end of the experiment the control device efficiency has decreased to ~12%, while PSC passivated with **V1336** retained majority of the performance and still showed the PCE of ~20%. There is a huge difference comparing both devices after 1000 h and the passivated it is obvious that the **V1336** significantly increases moisture stability.

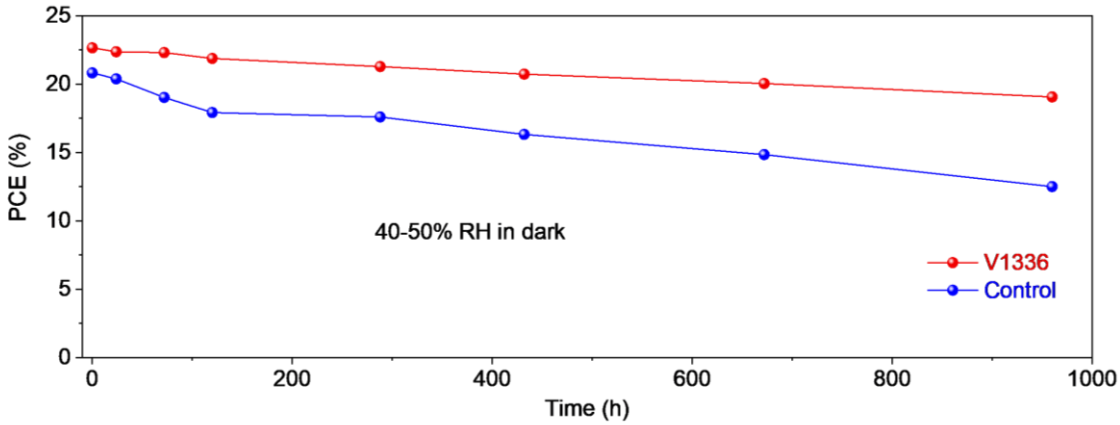

Figure 3.7. Stability test of V1336 passivated and control PSCs. The test was done in dark humid environment (40-50% RH).

3.2. Synthesis of perfluorinated diammonium cation with ethenyl linkers

Perfluorinated cation having ethenyl ammonium iodide linkers in *para*-position was synthesized in a four-step synthesis procedure (scheme **3.2.**).

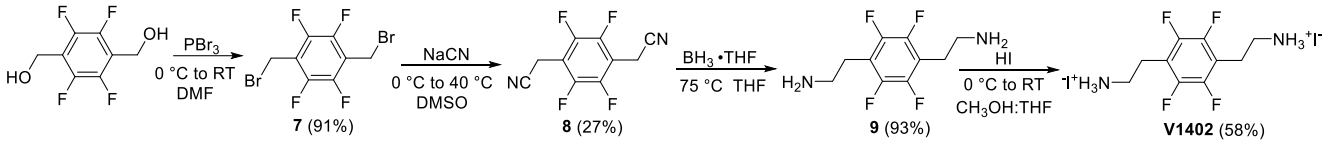

Scheme 3.2. Synthesis of 2,2'-(perfluoro-1,4-phenylene)bis(ethan-1-aminium) iodide (V1402)

The substitution reaction was conducted to substitute hydroxides with bromides. A solution of PBr_3 in CH_2Cl_2 was used as a brominating agent at 0°C under argon atmosphere to obtain .**(7)** in 91% yield, which was used to synthesize 2,2'-(perfluoro-1,4-phenylene)diacetonitrile **(8)**. After a number of failed attempts the goal was finally achieved by reaction of **7** in DMSO being added dropwise to the TFA/NaCN mixture while keeping external cooling [52]. Then, the desired product had the yield of only 27% because undesired products have been synthesized as well.

Afterwards, compound **8** was further used in reduction reaction to obtain 2,2'-(perfluoro-1,4-phenylene)bis(ethan-1-amine) **(9)** which had the yield of 93%. **8** was dissolved in THF and a solution of BH_3·THF was added dropwise under argon atmosphere and refluxed overnight.

Finally, compound **9** was dissolved in CH_3OH:THF (v:v, 1:1) and HI was added dropwise while the flask was in an ice bath. The final product 2,2'-(perfluoro-1,4-phenylene)bis(ethan-1-aminium) iodide **(V1402)** had the yield of 58%.

During each stage of the reactions, compounds **7**, **8** and the final product **V1402** were confirmed with ^{1}H, ^{13}C NMR spectra, elemental analysis and MS. Compound **9** was identified only with MS as typically primary amines may have stability problems.

The experiments with synthesized **V1402** haven't been conducted yet by the partners and it is still being tested. It is expected to show increased PCE and/or stability in PSCs since it is similar to **V1334**, which was the only one in the previous series to be successfully integrated in 2D PSC

structure. **V1402** also contains fluorine atoms, which are known to have hydrophobic properties and could increase moisture stability. As these are only speculations, precise results can only be analysed in the near future.

3.3. Synthesis of perfluorinated diammonium cation with methylene linkers

The last final product in this work was (perfluoro-1,4-phenylene)dimethanaminium iodide **(V1372)**. Two pathways were taken to obtain this product, because the yield in one stage were quite low (scheme **3.3.**). **V1372** was later used for further investigations to figure out if it might increase PCE.

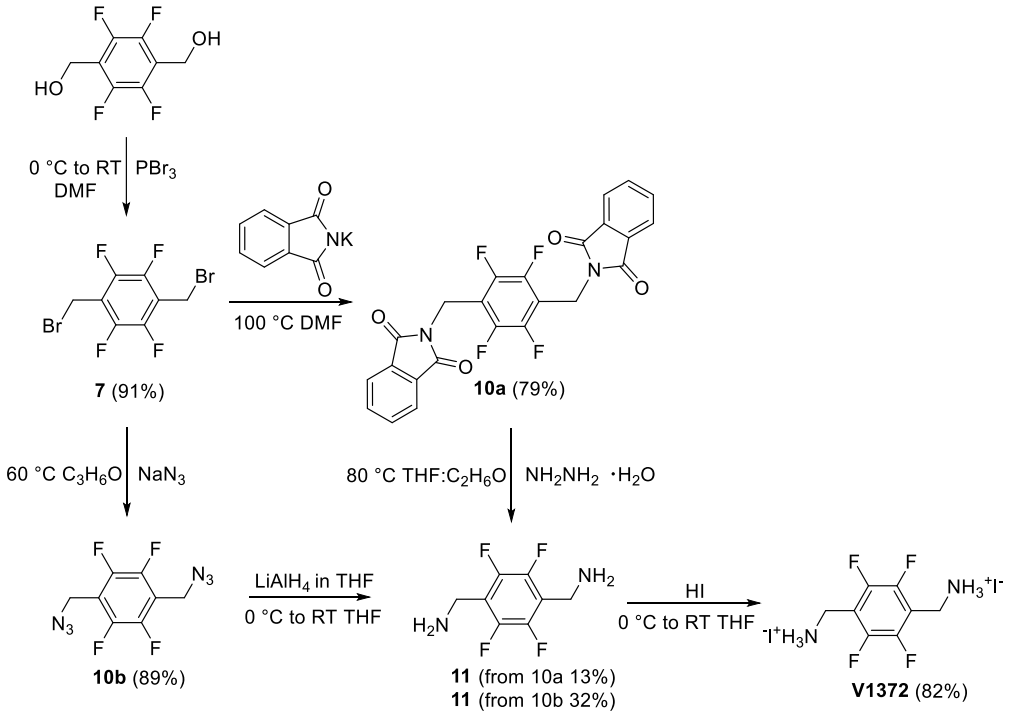

Scheme 3.3. Synthesis of (perfluoro-1,4-phenylene)dimethanaminium iodide (V1372)

In the beginning, the same compound **7** was used which was synthesized previously. **7** was used in Gabriel synthesis with potassium phthalimide to gain 2,2'-((perfluoro-1,4-phenylene)bis(methylene))bis(isoindoline-1,3-dione) **(10a)** with a yield of 79%. To a solution of **7** in DMF, potassium phtalimide was added and it was stirred at 100°C overnight. Later on, **10a** was dissolved in THF:EtOH (v:v; 1:1) and $NH_2NH_2 \cdot H_2O$ was added and the mixture was refluxed to obtain (perfluoro-1,4-phenylene)dimethanamine **(11)** with a quite low yield of 13%.

Since the yield of synthesized compound **11** was very low, another approach was taken. 1,4-bis(azidomethyl)-2,3,5,6-tetrafluorobenzene **(10b)** was synthesized while reacting **7** with NaN_3 to obtain **10b** with the yield of 89%.

Following the literature procedure describing reaction from **10b** to **11** with a promising yield of 93% it was expected to synthesize **11** with a similar yield [53]. However, after the reaction where **10b** was dissolved in THF and added dropwise to a solution of $LiAlH_4$ in THF at 0°C under argon atmosphere, gained yield was only 32%. Nevertheless, it was still better than synthesis from **10a**, where the yield was even lower – 13%.

After obtaining compound **11** from two different pathways, it was possible to synthesize desired product **V1372**. At first, **11** was dissolved in THF and the flask was placed in an ice bath where HI was added dropwise under argon atmosphere. The flask was covered and stirred overnight. After all, the final product of (perfluoro-1,4-phenylene)dimethanaminium iodide **(V1372)** was isolated in 82% yield.

After every synthesis of each compound **(10a, 10b, V1372)** they were confirmed with ^{1}H, ^{13}C NMR spectra, elemental analysis and MS. Compound **11** was only identified with MS because similarly to previously synthesized compounds **4**, **5**, **6** and **9** it also showed stability problems during the purification using column chromatography.

3.3.1. Performance evaluation of diammonium fluorous cation with methylene linkers

Synthesized **V1372** was tested if it could increase PSCs efficiency. Similar strategy as for isomeric cations described above was used. This organic spacer cation was used to passivate all-inorganic $CsPbI_3$ perovskite surface in a device architecture shown (figure **3.8.**). Afterwards, the control device without surface passivating cation was compared to PSC with passivated **V1372** on all-inorganic perovskite.

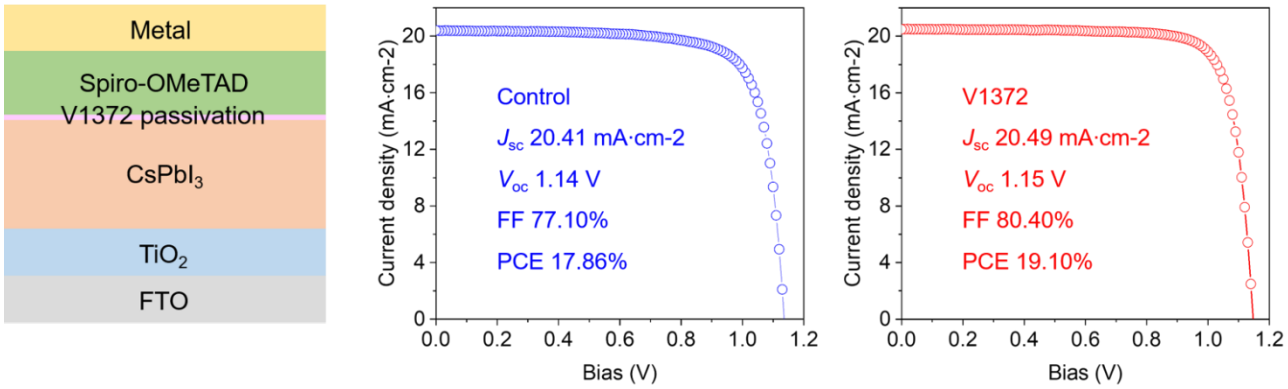

Figure 3.8. Device architecture used in a passivation study (left); *J-V* curves showing PSCs performance of control device without passivation (centre) and PSC with passivation of V1372 on all-inorganic perovskite (right).

Key parameters such as *Jsc*, *Voc*, FF and PCE were described. The preliminary data shows that the control device gives a PCE of 17.86%, whereas with passivated **V1372** cation the PCE was improved up to 19.10%. It is obvious that just by having **V1372** passivation on the perovskite the device gives a greater result, which means that **V1372** participates in boosting the efficiency. **V1372** lessens perovskites defects and suppresses recombination at the interface between the perovskite layer and HTL which resulted in improved device performance, which is one of the highest results employing all inorganic perovskite composition. Further device optimization and comparison with the **V1402** is needed for full evaluation of perfluorinated cations.

Conclusions

1. 1,3-phenylenediethanaminium iodide and 1,2-phenylenediethanaminium iodide cannot be incorporated in a two-dimensional perovskite solar cell upon mixing with the PbI_2 to function properly. It is due to steric hinderance since their substituents are in *meta*- and *ortho*-positions which are closer to each other in the benzene ring.
2. 1,4-phenylenediethanaminium iodide was successfully incorporated in a functional two-dimensional perovskite solar cell to have a power conversion efficiency of 13.54 % in reverse scan and 12.32 % in forward scan.
3. 1,4-phenylenediethanaminium iodide, 1,3-phenylenediethanaminium iodide and 1,2-phenylenediethanaminium iodide were successfully used as a passivation layers on top of three-dimensional perovskite solar cell. Only 1,2-phenylenediethanaminium iodide surpasses power conversion efficiency of the control three-dimensional perovskite solar cell by having 22.41±0.56 % whereas control reaches 20.88±0.60 %.
4. 1,2-phenylenediethanaminium iodide passivated PSC showed increased moisture stability. Control perovskite solar cell have lost power conversion efficiency by 9.94 % in 1000 hours affected by 40-50 % humidity while perovskite solar cell with 1,2-phenylenediethanaminium iodide passivation only lost 3.07 %.
5. (Perfluoro-1,4-phenylene)dimethanaminium iodide was successfully used for passivation on all-inorganic $CsPbI_3$ perovskite layer and it was further compared with control perovskite solar cell without the organic cation. When (perfluoro-1,4-phenylene)dimethanaminium iodide was used as passivation layer perovskite solar cell showed increased power conversion efficiency of 19.10 % compared to control perovskite solar cell – 17.86 % showing one of the best power conversion efficiency results for $CsPbI_3$ perovskite.

List of references

1. Sharma, S., Jain, K. and Sharma, A. Solar Cells: In Research and Applications—A Review. Materials Sciences and Applications, 6, 1145-1155. (2015) DOI: 10.4236/msa.2015.612113.
2. Corkish, R. Encyclopedia of Energy. Solar Cells. Pages 545-557, (2004) DOI: https://doi.org/10.1016/B0-12-176480-X/00328-4
3. Mathan K. P., Abinash D., Lalu S. and Ranjith G. N. Perovskite Photovoltaics. Chapter 8 - Fabrication and Life Time of Perovskite Solar Cells. Pages 231-287. (2018) DOI: https://doi.org/10.1016/B978-0-12-812915-9.00008-3
4. Snaith H. J. Present status and future prospects of perovskite photovoltaics. Nature Materials 17, 372-376(2018).
5. Yang Sh., Fu W., Zhang Zh., Chen H. and Li Ch-Zh. Recent advances in perovskite solar cells: efficiency, stability and lead-free perovskite. J. Mater. Chem. A, 2017,5, 11462-11482. (2017) DOI: https://doi.org/10.1039/C7TA00366H
6. Jeong, J., Kim, M., Seo, J. et al. Pseudo-halide anion engineering for α-FAPbI3 perovskite solar cells. Nature 592, 381–385 (2021). https://doi.org/10.1038/s41586-021-03406-5
7. Jiang X., Zhang J., Ahmad S., Tu D., Liu X., Jia G., Guo X and Li C. Dion-Jacobson 2D-3D perovskite solar cells with improved efficiency and stability. Nano Energy, Volume 35. (2020) DOI: https://doi.org/10.1016/j.nanoen.2020.104892
8. Belghachi A. Theoretical Calculation of the Efficiency Limit for Solar Cells. Laboratory of Semiconductor Devices Physics, University of Bechar, Algeria. (2015) DOI: 10.5772/58914
9. By Energy Concepts. How Does Solar Compare to Other Types of Energy? (2021) https://www.energyconceptsfresno.com/blog/2021/february/how-does-solar-compare-to-other-types-of-energy-/
10. Kibria T. M., Ahmmed A., Sony M. S., Hossain F. and Ul-Islam S. A Review: Comparative studies on different generation solar cells technology. (2014) Institute of Energy, University of Dhaka, Dhaka-1000, Bangladesh.
11. Khatibi A, Razi Astaraei F, Ahmadi MH. Generation and combination of the solar cells: A current model review. Energy Sci Eng. (2019);7:305–322. https://doi.org/10.1002/ese3.29
12. Nanalyze. Hialtek Organic Solar Cells Show Promise. (2013) [Accessed on April 28th, 2021] https://www.nanalyze.com/2013/10/heliatek-organic-solar-cells-show-promise/
13. Sinha S., Nandi D. K., Pawar P. S., Kim S. H., and Heo J. A review on atomic layer deposited buffer layers for Cu(In,Ga)Se2 (CIGS) thin film solar cells: Past, present, and future. (2020) https://doi.org/10.1016/j.solener.2020.09.022
14. Enkhardt S. CIGS cells could hit efficiencies of 33%, say Germany scientists. (2020) [Accessed on April 28th, 2021] From pv magazine, Germany.
15. Rahman A. M. Enhancing the photovoltaic performance of Cd-free Cu2ZnSnS4 heterojunction solar cells using SnS HTL and TiO_2 ETL. Bangladesh. (2021) DOI: https://doi.org/10.1016/j.solener.2020.12.020
16. Areffin U. A., Prianka K. T. K., Hosain B. M. and Snigdha H. A. Characterization and Analysis of Quantum-Dot PV Solar-Cells. (2016) http://dx.doi.org/10.13140/RG.2.1.3295.8488
17. Material District. Innovation: Thin Film Solar Cells At MX2016. Article (2016), [Accessed on April 28th, 2021] https://materialdistrict.com/article/innovation-thin-film-solar-cells-at-mx2016/

18. Alternative Energy Tutorials. Measuring the Power of the Solar Panel. I-V Characteristic Curves. (2020) [Accessed of April 28th, 2021] https://www.alternative-energy-tutorials.com/solar-power/measuring-the-power-of-a-solar-panel.html
19. Ossila. Solar Cells: A Guide to Theory and Measurement. https://www.ossila.com/pages/solar-cells-theory#:~:text=The%20key%20characteristic%20of%20a%20solar%20cell%20is,other%20useful%20metrics%2C%20current-voltage%20%28IV%29%20measurements%20are%20performed. [Accessed on April 28th].
20. Uddin M. H. Performance of Different DC/DC Converters for Maximum Power Point Tracking in Photovoltaic Systems. (2014) DOI:10.13140/RG.2.2.21137.38245
21. Sundaram, S., Benson, D. and Mallick, K. T. Solar Photovoltaic Technology Production. Chapter 2 – Overview of the PV Industry and Different Technologies. 2.4.3 Perovskite Solar Cells. Environment and Sustainability Institute, University of Exeter, United Kingdom (2016), Pages 7-22. DOI: https://doi.org/10.1016/B978-0-12-802953-4.00002-0
22. Kazim, S., Nazeeruddin, M., Gratzel, M., and Ahmad, S. Perovskite as Light Harvester: A Game Changer in Photovoltaics. Angewandte Chemie International Edition, 53(11), 2812-2824. (2014) doi:10.1002/anie.201308719
23. Chen, Y., Zhang, L., Zhang, Y., Gao, H. and Yan, H. Large-area perovskite solar cells – a review of recent progress and issues. RSC Adv.,2018,8, 1048 (2018). DOI: 10.1039/c8ra00384j
24. Rakstys, K., Igci, C. and Nazeeruddin, M. K. Efficiency vs. stability: dopant-free hole transporting materials towards stabilized perovskite solar cells. Chem. Sci., 2019,10, 6748-6769. (2019) https://doi.org/10.1039/C9SC01184F
25. Calio, L., Kazin, S., Gratzel, M. and Ahmad, S. Hole-Transport Materials for Perovskite Solar Cells. Angewandte Chemie International Edition, 55(47), 14522-14545. (2016) Doi:10.1002/anie/201601757
26. Ortiz-Cervantez, C., Carmona-Monroy, P. and Solis-Ibarra, D. Two-Dimensional Halide Perovskites in Solar Cells: 2D or not 2D? ChemSusChem. (2019) Doi:10.1002/cssc.201802992
27. Smith, I. C., Hoke, E. T., Solis-Ibarra, D., McGehee, M. D. and Karunadasa, H. I. A layered hybrid perovskite solar-cell absorber with enhanced moisture stability. Angewandte Chemie (International ed. in English), 53(42), 11232–11235. (2014). https://doi.org/10.1002/anie.201406466
28. Huang, Y., Li, Y., Lim, L. E., Kong, T., Zhang, Y., Song, J., Hagdeldt, A. and Bi, D. Stable Layered 2D Perovskite Solar Cells with an Efficiency of over 19% via Multifucntional Interfacial Engineering. J. Am. Chem. Soc. 2021, 143, 10, 3911-3917. (2021) DOI: https://doi.org/10.1021/jacs.0c13087
29. Sum, T. C. and Mathews, N. Advancements in perovskite solar cells: photophysics behind the photovoltaics. Energy Environ. Sci., 2014, 7, 2518-2534. (2014) DOI: 10.1039/C4EE00673A
30. Grancini, G. and Nazeeruddin, M. K. Dimensional tailoring of hybrid perovskites for photovoltaics. Nature Reviews Materials volume 4, pages4–22(2019). https://doi.org/10.1038/s41578-018-0065-0
31. Zhou, N., Huang, B., Sun, M., Zhang, Y., Li, L., Lun, Y., Wang, X., Hong, J., Chen, Q. and Zhou, H. The Spacer Cations Interplay for Efficient and Stable Layered 2D Perovskite Solar Cells. Advanced Energy MaterialsVolume 10, Issue 1 1901566 (2019). DOI: https://doi.org/10.1002/aenm.201901566

32. Li, H., Milic, V. J., Ummadisingu, A., Seo J. Y., Im, J. H., Kim, H. S., Liu, Y., Dar, M. I. et al. Bifunctional Organic Spacers for Formamidinium-Based Hybrid Dion−Jacobson Two-Dimensional Perovskite Solar Cells. Nano Lett. 2019, 19, 150-157. DOI: https://pubs.acs.org/doi/10.1021/acs.nanolett.8b03552
33. Ruddlesden, S. N. and Popper, P. The compound Sr3Ti2O7 and its structure. Acta Crystallographica, 11(1), 54-55. (1957) doi:10.1107/s0365110x58000128
34. Xu, X., Pan, Y., Zhong, Y., Ran, R. and Shao, Z. Ruddlesden-Popper Perovskites in Electrocatalysis. Materials Horizons. (2020) Doi:10.1039/d0mh00477d
35. Mao, L., Stoumpos, C. C. and Kanatzidis, M. G. Two-Dimensional Hybrid Halide Perovskites: Principles and Promises. J. Am. Chem. Soc. 2019, 141, 1171-1190. DOI: http://dx.doi.org/10.1021/jacs.8b10851
36. Ducinskas, A., Kim, G. Y., Moia, D., Senocrate, A., Wang, Y. R., Hope M. A., Mishra. A et al. Unravelling the Behavior of Dion−Jacobson Layered Hybrid Perovskites in Humid Environments. ACS Energy Lett. 2021, 6, 337-334. DOI: https://dx.doi.org/10.1021/acsenergylett.0c02344?ref=pdf
37. Ahmad, S., Fu, P., Yu, S., Yang, Q., Liu, X., Wang, X., Guo, X. et al. Dion-Jacobson Phase 2D Layered Perovskites for Solar Cells with Ultrahigh Stability. Joule. Volume 3, Issue 3, 20 March 2019, Pages 794-806. (2019) DOI: https://doi.org/10.1016/j.joule.2018.11.026
38. Ma, S., Cai., M., Cheng, T., Ding, X., Shi, X., Alsaedi, A., Hayat, T. et al. Two-dimensional organic-inorganic hybrid perovskite: from material properties to device applications. Science China Materials volume 61, pages1257–1277(2018). DOI: https://doi.org/10.1007/s40843-018-9294-5
39. Al-Ahouri A., Kohnen E., Magomedov A., Getautis V., Caprioglio P. et al. (2020) Monolithic perovskite/silicon tandem solar cell with >29% efficiency by enhanced hole extraction. Science 370(6522). DOI:10.1126/science.abd4016
40. Jiang, X., Chen, S., Li, Y., Zhang, L., Shen, N., Zhang, G., Du, J. et al. Direct Surface Passivation of Perovskite Film by 4-Fluorophenethylammonium Iodide toward Stable and Efficient Perovskite Solar Cells. ACS Appl. Mater. Interfaces 2021, 13, 2, 2558–2565. DOI: https://doi.org/10.1021/acsami.0c17773
41. Huang, P., Kazim, S., Wang, M. and Ahmad, S. Toward Phase Stability: Dion−Jacobson Layered Perovskite for Solar Cells. ACS Energy Lett. 2019, 4, 2960-2974. DOI: http://dx.doi.org/10.1021/acsenergylett.9b02063
42. Jiang, X., Zhang, J., Ahmad, S., Tu, D., Liu, X., Jia, G., Guo, X. and Li, C. Dion-Jacobson 2D-3D perovskite solar cells with improved efficiency and stability. Nano Energy 75 (2020) 104892. DOI: https://doi.org/10.1016/j.nanoen.2020.104892
43. Ma, C., Shen, D., Ng, T.-W., Lo, M.-F. and Lee, C.-S. 2D Perovskites with Short Interlayer Distance for High-Performance Solar Cell Application. Advanced Materials, 30(22), 1800710. (2018) doi:10.1002/adma.201800710
44. Garcia-Benito, I., Quarti, C., Queloz, V. I. E., Orlandi, S., Zimmermann, I., Cavazzini, M., Lesch, A. Et al. Fashioning Fluorous Organic Spacers for Tunable and Stable Layered Hybrid Perovskites. Chem. Mater. 2018, 30, 8211-8220. DOI: http://dx.doi.org/10.1021/acs.chemmater.8b03377

45. Lu, D., Lv, G., Xu, Z., Dong, Y., Ji, X. and Liu, Y. Thiophene-based Two-Dimensional Dion–Jacobson Perovskite Solar Cells with over 15% Efficiency. J. Am. Chem. Soc. DOI: 10.1021/jacs.0c03363
46. Garziano, L., Stassi, R., Macri, V., Stefano, O. D., Savasta, S. and Nori, F. One Photon Can Simultaneously Excite Two or More Atoms.2016, Physical Review Letters 117(4). DOI: 10.1103/PhysRevLett.117.043601
47. Mao, L., Stoumpos, C. C. and Kanatzidis, M. G. Two-Dimensional Hybrid Halide Perovskites: Principles and Promises. (2019) http://pubs.acs.org/action/showCitFormats?doi=10.1021/jacs.8b10851
48. Lee, J.-W., Dai, Zh., Han T.-H., Choi, C., Chang, Sh.-Y., Lee, S.-J., De Marco, N., Zhao, H., Sun, P., Huang, P. and Yang Y. 2D perovskite stabilized phase-pure formamidinium perovskite solar cells. Nature Communications volume 9, Article number: 3021 (2018). DOI: https://doi.org/10.1038/s41467-018-05454-4
49. Wang, X., Rakstys, K., Jack, K. et al. Engineering fluorinated-cation containing inverted perovskite solar cells with an efficiency of >21% and improved stability towards humidity. Nat Commun 12, 52 (2021). DOI: https://doi.org/10.1038/s41467-020-20272-3
50. Moreau, J. J. E., Pichon, B. P., Bied, C. and Man, M. W. C. (2005). Structuring of bridged silsesquioxanes via cooperative weak interactions: H-bonding of urea groups and hydrophobic interactions of long alkylene chains. Journal of Materials Chemistry, 15(35-36), 3929. Doi:10.1039/b504635a
51. Fu, W., Chen, H. and Jen, A. K.-Y. Two-dimensional perovskites for photovoltaics. Materials Today Nano. Volume 14, 2021, 100117. DOI: https://doi.org/10.1016/j.mtnano.2021.100117
52. Kalir, A., and Mualem, R. (1987). One-Step Synthesis of 2- and 4-Nitrobenzyl Cyanides. Synthesis, 1987(05), 514-515. Doi:10.1055/s-1987-27989
53. Okamoto, H., Kozai, T., Okabayashi Z., Shinmyozu, T., Ota, H., Amimoto, K. and Satake, K. Synthesis, structure, and photoreactions of fluorinated 2,11-diaza[32]paracyclophane: Photochemical formation of cage-diene type benzene dimer. Journal of Physical Organic Chemistry Volume 30, Issue 9 e3726. (2017). DOI: https://doi.org/10.1002/poc.3726

List of publications

R. Skačkauskaitė, K. Rakštys. Synthesis of divalent organic cations and their application in highly efficient and stable perovskite solar cells. Conference presentation materials from “Chemistry and chemical technology 2021”; Kaunas, 2021.

S. Driukas, G. Kavaliauskaitė, **R. Skačkauskaitė**, K. Rakštys, M. Franckevičius ir V. Gulbinas. Passivation of $FA_{0.95}Cs_{0.05}PbI_3$ Perovskite with (phenylene)di(ethylammonium) orto-, meta-, para- Cations Improves Charge Carrier Extraction. Open Readings. 2021.

Acknowledgments

My cordial thanks to **Dr. K. Rakštys** for passing onto me a great amount of knowledge and skills as well as his patience and all-around support in realizing this work.

I express my gratitude to **Prof. Dr. V. Getautis** for the given opportunity to work in his research group.

I thank **Dr. M. Daškevičienė** for being my supervisor and for her support.

I would also like to thank my fellow students and colleagues **Doct. D. Vaitukaitytė**, **A. Drevilkauskaitė**, **P. Luižys** for creating an enjoyable working atmosphere and many interesting conversations.

I am grateful to all the research group and people who participated in providing certain results from various methods.